Evolutionary analysis of THAP9 transposase: conserved regions, novel motifs

Richa Rashmi[1], Chandan Nandi[1], Sharmistha Majumdar[1]

[1]Discipline of Biological Engineering, IIT Gandhinagar

Abstract

THAP9 is a transposable element-derived gene that encodes the THAP9 protein, which is homologous to the *Drosophila* P-element transposase (DmTNP) and can cut and paste DNA. However, the exact functional role of THAP9 is unknown. Here, we perform evolutionary analysis and extensive *in silico* characterization of THAP9, including predicting domains and putative post-translational modification sites. We predict previously unreported mammalian-specific post-translational modification sites that may play a role in the subcellular localization of THAP9. We also observe that although THAP9 has evolved under a strong pervasive purifying selection, yielding high conservation of THAP9, there are distinct class-specific conservation patterns of key functional residues in certain domains. Furthermore, investigation of THAP9 expression profiles in various cancer and matched normal datasets demonstrated underexpression and overexpression in testicular cancers and thymic epithelial tumors, respectively, thus suggesting a possible role of THAP9 in cancer.

Keywords

Evolutionary analysis; Transposase gene; Role in cancers, Protein sequence characterization

Introduction

Transposable elements (TEs) are DNA sequences that can move and duplicate within a genome[1]. They can cause various mutations as well as an increase in genome size[2]. Thus, TEs, which constitute 25% - 50% of various genomes, play a significant role in evolution.

Many genes are derived from transposable elements. Human THAP9, which encodes the hTHAP9 protein, is one such gene. The hTHAP9 protein is a homolog of the Drosophila P-element transposase (DmTNP) (more than 25% homology)[3]. The DmTNP protein mobilizes the P-element transposon, which is the causative agent for hybrid dysgenesis in Drosophila[4].

hTHAP9 belongs to the THAP (Thanatos-associated protein) protein family in humans, with twelve proteins (hTHAP0-hTHAP11). All human THAP proteins are characterized by an amino-terminal DNA-binding domain called the THAP domain, which is typically 80-90 amino acid residue-long and possesses a C2CH type Zinc Finger[4,5].

Many THAP family proteins are known to be involved in various human diseases. THAP1 is involved in torsional dystonia and hemophilia[6], THAP5 is involved in heart diseases[7], THAP2[8], THAP10[9], and THAP11[10] are involved in multiple cancers. Also, the THAP9-AS1 gene, which is

the neighboring gene in the 5' upstream region of THAP9, is overexpressed in pancreatic cancer[11]. Moreover, according to NCBI & the Protein Atlas, THAP9 has high expression in the brain, ovary, prostate, testis & thyroid (https://www.ncbi.nlm.nih.gov/gene/79725, https://www.proteinatlas.org/ENSG00000168152-THAP9/tissue). Nevertheless, the exact functional role of THAP9 and its association with various diseases remains unknown.

Phylogenetic analysis and evolutionary tests of hTHAP9 can help us understand the evolution and the type and extent of natural selection for the hTHAP9 gene and its associated protein. In the course of evolution, negative or purifying selection is used to eliminate unfavorable and harmful mutations[12]. On the other hand, positive or diversifying selection leads to molecular adaptation by promoting favorable mutations[12]. Here, we present the evolutionary analysis and extensive *in silico* characterization, including predicting domains and putative post-translational modification sites for THAP9 and its orthologs. This study identified some previously unreported functional features in the THAP9 protein sequence, highly conserved in mammals. These include four adjacent motifs: N-glycosylation site, Protein kinase C (PKC) phosphorylation site, Leucine zipper domain, and Bipartite nuclear localization signal (NLS), which may play a role in the subcellular localization of THAP9. The study also revealed two N-myristoylation sites within the THAP domain. Moreover, it was observed that THAP9 has evolved under a strong pervasive purifying selection.

Materials and Methods

Identification of orthologs.

THAP domain containing 9 (*THAP9*) transcript variant 1 (RefSeq: NM_024672.6) from *Homo sapiens* was used to identify the orthologs from the Eukaryotic Genome Annotation pipeline of the NCBI database (National Center for Biotechnology Information, https://www.ncbi.nlm.nih.gov/) using a combination of protein sequence similarity and local synteny information for the available sequences. *hTHAP9* orthologs are present in 216 organisms, including 74 birds, 4 alligators, 7 turtles, 6 lizards, 4 amphibians, 120 mammals, and 1 lamprey. We used the following five representative classes: amphibians, hyperoartia, reptiles, birds, and mammals for comparison and representation purposes.

Sequence alignment & Phylogenetic analysis

A phylogeny-aware sequence alignment was performed for amino acid sequences using the CLUSTALW[13] method present in MEGAX[14] software using the guide trees generated from TimeTree[15] (http://www.timetree.org/). We created multiple sequence alignments (MSA) separately for all vertebrate classes (birds, alligators, turtles, lizards, amphibians, and mammals) and combined all species. Following the protein MSA of the orthologs, the Coding DNA Sequences (CDS) were codon aligned using PAL2NAL[16] (http://www.bork.embl.de/pal2nal/). Divergent sequences which created alignment errors were identified and removed manually. The codon alignments and the protein alignments were used to generate the maximum-likelihood tree using MEGAX with 100 bootstrap replicates, and the tree was visualized using iTOL[17].

Analysis for Selective Pressure

To characterize the selection patterns on the alignments of THAP9, we used various tools from the HyPhy package[18] implemented on the Galaxy webserver[19]. With the user-friendly graphical interfaces, new fast methods, and multi-tasking abilities, HyPhy provides better analysis power to users than the PAML[20] software package. The Galaxy web-server version of HyPhy provides additional advantages (e.g., it does not require any local installation, and we can automate the whole process by creating a workflow). The approximately-maximum-likelihood phylogenetic trees generated using FASTTREE[21] also implemented on Galaxy webserver were selected with the HyPhy model selection tool and the codon alignment file. For the HyPhy software package analysis, the default set parameters of p-values/posterior probabilities were considered. FEL[22] (Fixed Effect Likelihood) and FUBAR[23] (Fast Unbiased Bayesian AppRoximation) were utilized to identify sites evolving under pervasive diversifying and pervasive purifying selection pressures. MEME[24] (Mixed Effects Model of Evolution) was used to identify episodically diversifying sites. FEL is an ML-based model which assumes constant selection pressure on each site. The FUBAR model estimates site-by-site ω values while MEME allows the distribution of ω to vary over sites and additionally from branch to branch. Significance was assessed by posterior probability > 0.9 (FUBAR) and p-value < 0.1 (MEME) and p-value < 0.1 (FEL)[25].

Protein sequence characterization

The domain architecture of hTHAP9 and orthologs was predicted using SMART[26] (Simple Modular Architecture Research Tool, http://smart.embl-heidelberg.de/) in "batch mode" considering the option for including Pfam[27] domains. ELM[28] Prediction tool (Eukaryotic Linear Motif, http://elm.eu.org/) was used to identify short linear motifs using the fasta file containing hTHAP9 & the ortholog protein sequence as input. Furthermore, the previously unidentified conserved motifs and functional domains were searched using Meme-Suite[29] and ScanProsite[30], respectively. Disordered binding regions (DBR)[31] and secondary structure elements of the hTHAP9 protein were predicted using PSIPRED Workbench[32], and areas with disorder scores greater than 0.6 were considered as disordered. The physiochemical attributes of the hTHAP9 protein sequence such as molecular weight, theoretical pI, amino acid composition, atomic composition, extinction coefficient, estimated half-life, instability index, aliphatic index, and grand average of hydropathy (GRAVY) were computed using Expasy ProtParam[33] and EMBOSS Pepstats[34] (https://www.ebi.ac.uk/Tools/seqstats/emboss_pepstats/). We also analyzed the evolution of some previously reported functional domains and residues of hTHAP9 protein sequence individually, which includes THAP-domain, Leucine Zipper domain, Insertion domain & putative Catalytic Residues. Finally, previously annotated SMART & Pfam domains and newly predicted domains of hTHAP9 and its orthologs were visualized using iTOL[17].

Distribution of SNPs and mutations in cancer

The 1000 Genomes project[35] data using Ensembl[36] (reference genome: GRCh38.p13) was searched for missense mutations of hTHAP9 (ENSG00000168152). PolyPhen-2[37] scores given on the Ensembl result table were used to classify the SNPs into "benign," "possibly damaging,", "probably damaging". PolyPhen-2 predicts the effect of an amino acid substitution on the structure and function of a protein using sequence homology, Pfam annotations, 3D structures from PDB were available, and several other databases and tools (including DSSP, ncoils, etc.)[38]. Cancer-related missense mutations in THAP9 were identified using cBioPortal[39] for Cancer Genomics (http://www.cbioportal.org/). PolyPhen2 scores for these mutations were calculated

by submitting their genomic coordinates (for GRCh37 reference genome) to the Ensembl Variant Effect Predictor tool[40] (https://www.ensembl.org/Tools/VEP).

Cancer expression databases and web tools

To get an idea about the expression profile of the *hTHAP9 gene* in various cancers, we used the expression data from TCGA[41] (https://cancergenome.nih.gov) and GTEx[42] (https://gtexportal.org/home). Cancer and matched normal datasets from the above databases were accessed and plotted using the GEPIA[43] web server (http://gepia.cancer-pku.cn).

Results

Evolution of THAP9 through organisms

To study the possible functional role of hTHAP9, we conducted an extensive characterization of its protein sequence and investigated its evolution. hTHAP9 protein is encoded by the gene with the same name and is found on chromosome 4 in humans. Transcript variant 1 of hTHAP9 is known to encode the transposase protein[44]. Therefore, we used the same transcript variant for our analysis.

According to NCBI (Jan 2021), hTHAP9 protein has orthologs in 216 vertebrate organisms, including 74 birds, 4 alligators, 7 turtles, 6 lizards, 4 amphibians, 120 mammals, and 1 lamprey. We downloaded the protein & coding DNA sequences for the same from NCBI. We began our analysis by aligning the protein sequences using CLUSTALW[13] in a phylogeny-aware manner. We created the time tree for the organisms using timetree[15]. Post-alignment, we filtered the diverse, low-quality, and partial sequences, after which we were left with 178 sequences (3 amphibians, 1 hyperoartia, 13 reptiles, 53 birds,108 mammals). Later we realigned the sequences using CLUSTALW[13], followed by building Maximum likelihood Phylogenetic trees[45] with 100 bootstrap replicates. Both these parts were performed using options available in MEGAX[14]. We codon aligned the coding sequences from the orthologs using PAL2NAL[16], taking corresponding aligned protein sequences as input. The resulting trees (**Figure 1**) were drawn using the iTOL[17] web server. Rooting trees to the midpoint perfectly aligns the lamprey (hyperoartia), amphibians, reptiles, birds, and mammals in the given order, thus suggesting that THAP9 evolved with the evolution of the organisms, both at the level of DNA (**Figure 1b**) as well as the corresponding amino acid sequence (**Figure 1a**) of the gene.

Several types of tests can be used to speculate about the type and extent of natural selection. Negative or Purifying selection is used to eliminate unfavorable or deleterious mutations. It is mostly observed in housekeeping and essential genes. On the other hand, positive or diversifying selection favors mutations required for molecular adaptation and is mostly observed in genes involved in immunity, reproduction, and sensory systems. Random mutations or selective pressure that mutates gene sequences can cause either silent/ synonymous or non-synonymous mutations[46] due to degeneracy of the genetic code[51]. The rates of these two types of mutations are denoted as dS and dN, respectively, and their ratio is denoted as (omega); =dN/dS. Thus the value acts as an indicator of how natural selection has acted on the protein. Sites under diversifying/positive selection have a higher rate of non-synonymous

mutations and have a value greater than 1. If the site has a higher rate of synonymous mutations, it is under purifying/negative selection and bears a value less than 1. The tools used in our analysis used mathematical models to measure the values for each codon site across the length of the coding DNA sequence by comparing it with the orthologs[47].

To explore variations in selective pressures across THAP9, we used the HyPhy software[18] package available at Galaxy[19] web-server. Our analysis was aimed at the detection of selection at the individual codon level. We used HyPhy-FEL[22](Fixed Effect Likelihood), HyPhy-FUBAR[23] (Fast Unconstrained Bayesian AppRoximation), and HyPhy-MEME[24] (Mixed Effect Likelihood Model) to the codon-aligned sequence file from PAL2NAL[16]. All three methods employ a distinct algorithmic approach to infer selection. FEL uses maximum likelihood to fit a codon model to each site, thereby estimating a value for dN and dS at each site. FUBAR uses the Bayesian approach to selection inference. It uses *a* priori specified grid of dN and dS values (typically 20×20), spanning the range of negative, neutral, and positive selection regimes, whose likelihoods can be pre-computed and used throughout the analysis. MEME employs a mixed-effects maximum likelihood approach, where it infers two ω rate classes for each site and corresponding weights representing the probability that the site evolves under each rate class at a given branch[25].

FEL and FUBAR identified codon sites that evolved under the influence of pervasive (consistently across the entire phylogeny) diversifying and purifying selection, with p-value < 0.1 and posterior probability > 0.9, respectively. FEL predicted 8 diversifying sites and 514 purifying selected sites (**Figure 2 (a)**). Similarly, FUBAR predicted 1 diversifying selected sites and 618 purifying sites (**Figure 2 (b)**). By combining the results, we can say that THAP9 had been subjected to a strong negative selection, with one common positively selected site at Ile829 reported by both FEL and FUBAR.

MEME identifies site(s) in a gene subjected to both pervasive or episodic (only on a single lineage or subset of lineages) diversifying selection[25]. 197 codon sites (**Supplementary Table 1** https://docs.google.com/spreadsheets/d/1PJQu_fhi2EGv0MyaZHebu1_swTksFNDZG_aEVMTOwgU/edit#gid=1057877600) distributed across hTHAP9 were observed to have evolved under episodic diversifying selection through this analysis (**Figure 2 (c)**).

Based on the results from all 3 methods, we can say that THAP9 has evolved under a strong negative selection suggesting that THAP9 may have some stringent functional or structural requirements. The presence of many episodic positively selected sites suggests that certain essential mutations were favored across some lineages. Moreover, there was only one common positively selected site at Ile829 detected by all three methods.

Analysis of THAP9 protein orthologs suggests new functional motifs in mammals.

The physicochemical properties and domain architecture of THAP9 protein orthologs were predicted using various tools.

Physicochemical properties of hTHAP9: We predicted the physicochemical properties using Expasy ProtParam[33] and EMBOSS Pepstats[34]. hTHAP9 protein is a 903 amino acid long protein

with a molecular weight of 103410.79 Da. The isoelectric point (pI) of hTHAP9 is 9.4853. The instability index (Proteins having instability index<40 are considered stable) of hTHAP9 is 38.49 . The GRAVY value of hTHAP9 is -0.179, which predicts better interaction between the protein and water. The amino acid composition of hTHAP9 is shown in **Figure 3**.

Domain architecture: According to SMART[26] & Pfam[27], *hTHAP9* has an 89 residue-long THAP-type Zinc Finger domain at the N-terminal end followed by a 177 residue-long P-element transposase domain (Tnp_P_element, Pfam ID: PF12017) between residues 142 to 389 (**Figure 4**). SMART also predicted two low complexity regions in the h*THAP9* protein sequence from residues 444 to 455 and 567 to 579. Most of the THAP9 orthologs have similar SMART & PFAM annotations. All the annotated THAP9 ortholog sequences have the Tnp_P_element domain. However, some species lack the THAP domain, for example, *Falco Peregrinus* (Aves) and *Alligator Sinensis* (Reptile) (**Figure 4,** full representation in **Supplementary Figure 1(a)**). There are no THAP9 orthologs of Amphibians and Hyperoartia class with already annotated SMART or Pfam domains.

Functional Motifs: Various new functional features of THAP9 were predicted using the Eukaryotic Linear Motif[28] (ELM) and ScanProsite[30] (**Figure 5,** full representation in **Supplementary Figure 1(b)**).

3 N-myristoylation sites (Prosite ID: PS00008) were predicted in hTHAP9, namely (i) "GAilCS" located between residues 58 to 63, (ii) "GAvpSV" located between residues 83 to 88, and (iii) "GVsvTK" located between residues 679 to 684. The first two N-myristoylation sites are located in the N terminal THAP domain. hTHAP9 may localize to the nucleus as it has a sequence-specific DNA binding THAP domain[4,5] as well as a predicted bipartite NLS[48] (Figure 6). However, myristoylation is a protein-lipid modification essential for cellular signaling, protein-protein interactions as well as intracellular targeting of proteins to endomembrane or plasma membrane systems[49]. Thus, it is possible that THAP9 could also localize to cytosolic locations via selective myristoylation.

Moreover, the ELM and ScanProsite analysis also predicted the occurrence of 4 adjacent motifs located between 125 to 166, namely (i) "NYSL" N-glycosylation site (PS00001) from 125 to 128 (ii) "SIK" Protein kinase C phosphorylation site (PS00005) from 127 to 129 (iii) “LtigaekLaevqqmLqvskkrL” Leucine zipper pattern (PS00029) from 132 to 153 (iv) “KRLISVKNYR-MIKKRK" Bipartite nuclear localization signal profile (PS50079) from 151 to 166. This pattern is highly conserved in mammals (**Figure 6, Supplementary Figure 1(b)**).

Multiple previously unreported functional motifs (**Supplementary Table 2**) were also predicted. These motifs can be explored further to understand the regulation and function of THAP9.

NLS: NLS sequences generally appear either as a single-stretch (monopartite) or as two clusters (bipartite) of basic residues separated by approximately ten amino acid residues, with the respective consensus sequences being (K/R)4–6 and (K/R)2 X10–12(K/R)3[50]. ELM and ScanProsite analysis found a 16 residue long bipartite NLS sequence "KRLISVKNYR-MIKKRK," in which 50% of the residues were basic, and the basic region was more concentrated in the C-Terminal end of the motif.

Bipartite nuclear localization signals (NLS) are sometimes located close to (e.g., HSF2[51]) or within (e.g., SREBP-2 [52]) a Leu-zipper domain. Moreover, the subcellular localization of a protein may be regulated by masking and unmasking of its NLS by local phosphorylation events[52]. It is tempting to speculate that the subcellular localization of hTHAP9 may be regulated by its Leucine zipper domain which contains a bipartite NLS as well as a highly conserved Protein kinase C phosphorylation site.

Phosphorylation sites: Several kinase phosphorylation sites (Protein kinase C & Casein kinase II) were predicted to be distributed across the length of the protein. ELM also predicted one Host Cell Factor-1 binding motif in hTHAP9 that has been previously annotated[28,48].

Other domains: When we looked for weak domain matches in THAP9, ScanProsite also predicted the presence of a Phosphatase tensin-type domain profile (PPASE_TENSIN). Tumor suppressor protein PTEN is the best-characterized member of the PPASE_TENSIN family[53]. To further explore the weak presence of the PPASE_TENSIN (Prosite Entry: PS51181) domain in the human THAP9 protein, we looked for this domain in all the THAP9 ortholog sequences using ScanProsite (Option 3). The PPASE_TENSIN domain was identified in 105 orthologs.

The Phosphatase tensin-type domain is present in 38 protein sequences in the Uniprot database[54], including human PTEN. To look for conserved motifs in the predicted PPASE_TENSIN domain sequences in 105 THAP9 orthologs and the 38 proteins from Uniprot, we processed them through the MEME tool part of the MEME-Suite[29] using site distribution parameter as "one occurrence per sequence." We identified 15 highly conserved motifs, but the confidence score of these matches was not significant enough.

To further examine the diversification of THAP9 orthologs, we predicted conserved motifs using MEME[29]. We identified the distribution of the top 30 conserved motifs occurring at least once in all the sequences (**Figure 7; Table 1**). The motif composition appeared more conserved in mammals than other groups, suggesting functional relevance in mammals as well as functional diversification among other classes.

Evolution of individual domains.

To study the functional diversification of THAP9 among different vertebrate classes in more detail we studied the evolution of some previously reported functional domains and residues of functional relevance. We looked at the evolution of the THAP domain, L-Zipper domain, predicted insertion domain as well RNaseH-like catalytic domain[55] (including 8 putative catalytic residues namely K282, D304, D374, D414, D519, E613, D695, E776 in hTHAP9) in 178 orthologs.

THAP-Domain: The THAP domain, the characteristic feature of the THAP family proteins, is a conserved 80-90 amino acid DNA binding domain located at the N-terminal end of the protein. The THAP domain is a C2CH type Zinc Finger domain that can bind specific DNA sequences and has a conserved secondary structure, namely a characteristic β-α-β fold with four loops (L1-L4) interconnecting the sheets and the helix[5].

Our analysis showed that the THAP-Domain is present in all amphibian (3) and hyperoartia (1) orthologs and in most orthologs in reptiles (12 out of 13), birds (26 out of 53), and mammals (105 out 108). The THAP domain shows high conservation within these organism classes (**Figure 8, Supplementary Table 3**). In a few organisms, the THAP domain was truncated (N Terminal deletion: *Apteryx rowi, Piliocolobus tephrosceles, Tupaia Chinensis*; C Terminal deletion: *Haliaeetus leucocephalus, Chinchilla lanigera, Puma concolor*).

Structure-based multiple sequence alignment of the THAP domains of DmTNP, human THAP1, 2, 7, 9, and 11, and C. elegans CtBP by Sabogal et al.[4] reported the conservation of zinc-coordinating C2CH motif and base-specific DNA-binding residues (corresponding hTHAP9 residues are C5, C10, C62, H65, P29, W38, V85, and P86 (* marked in **Figure 8**). We investigated the conservation of these residues across the THAP9 orthologs. It was observed that within the 147 orthologs containing THAP domains, C5 is conserved in 142 orthologs (mutated in 3 mammals and 2 aves), C10 is conserved in 141 orthologs (mutated in 4 mammals and 2 aves), C62 is conserved in 144 orthologs (mutated in 2 mammals and 1 aves), H65 is conserved in 143 orthologs (mutated in 3 mammals and 1 aves), V85 is conserved in 137 orthologs (mutated in 2 mammals, 1 aves, 4 reptiles, and 3 amphibians), P86 is conserved in 144 orthologs (mutated in 2 mammals and 1 aves). Interestingly, P29 and W38 are conserved in all 147 orthologs. Moreover, the THAP domain showed a distinct pattern within bats, camels, whales, rodents & lizards (**Supplementary Table 3**).

Leucine Zipper Domain: hTHAP9 has a ~40 amino acid long leucine-rich region located downstream of the DNA-binding THAP domain[56]. This was corroborated by our ScanProsite analysis which also predicted a highly conserved L-Zipper domain in the same region. Several DNA transposases like DmTNP[57], IS911[58] and KP repressor[59] (inhibitor of DmTNP) form multimers using the leucine zipper region. In another study, it was observed that mutating the leucines (L90, L128, L132, L139, L146, and L153 to Ala, either individually or together) or deleting the leucine-rich predicted coiled-coil region in hTHAP9 did not disrupt homo-oligomerization[48]. This suggests that maybe THAP9 utilizes a multidomain mechanism for oligomerization. So, we decided to look at the evolution of the L-Zipper domain of THAP9 to get a further understanding of its conservation.

We observed that the L-Zipper Domain is not present in any of the amphibians, hyperoartia, and reptilian orthologs of THAP9. Moreover, it is only present in 14 out of 53 Aves orthologs and 91 out of 108 mammalian orthologs. Thus, it is interesting to note that the L-Zipper domain appeared much later during vertebrate evolution and is highly conserved across mammals. Moreover, L132, L139, L146, and L153 (residue numbers correspond to hTHAP9, **Supplementary Table 4,** highlighted with * in **Figure 9**) are conserved in all the orthologs in which L-Zipper is detected.

RNase-H-like fold: A recent study[55] predicted an RNase-H-like fold in hTHAP9 using secondary structure predictions, homology modeling, and multiple sequence alignment. The RNase-H fold brings three catalytic residues (DDD/E) in close proximity, which coordinate with two divalent metal ion cofactors (mostly Mg2+) to form the active site for DNA cleavage and strand transfer during transposition[60,61]. RNase-H fold-containing proteins are generally multi-domain in nature with domains involved in sequence-specific DNA binding and multimerization in addition to the RNaseH-like catalytic domain[55,57,62]. The study experimentally confirmed that D304, D374, and E613 are important catalytic residues responsible for DNA excision[52]. The catalytic triad of DmTNP is formed by D230, D303 & E531. It was observed that D374 and E613 of hTHAP9 align with D303 and E531 catalytic residues of DmTNP. But D304 of hTHAP9 does not align with D230 of DmTNP, instead, D230 of DmTNP aligns with K282 of hTHAP9. Moreover, they also observed that besides the predicted catalytic triad, there were other conserved acidic

residues in the signature string of hTHAP9, which were important for DNA transposition including D414, D519, and D695. They also predicted that the RNase-H fold in hTHAP9 appears to be disrupted by an insertion domain between S415 to T604, similar to the insertion domain of DmTNP[57] which binds GTP via GTP-binding motifs. Despite the disruption of the RNase-H fold, both DmTNP and hTHAP9 are able to cut the substrate DNA[55,57].
We investigated the evolution of these important catalytic residues i.e. K282, D304, D374, D414, D519, E613, D695 & E776 (**Figure 10, Supplementary Table 5**). Interestingly K282 was observed to be D in 2 out of 3 Amphibians and D in the hyperoartia. Moreover, out of 13 reptiles, it was A in 1, D in 2, G in 3, and E in 7. But K282 was Q in 51 out 53 birds and K in 107 out of 108 mammals. With this, we can speculate that over the course of evolution the catalytic residue D got changed to K which possibly contributed to the hindered transposition mechanism of hTHAP9 and thus led to the domestication of hTHAP9. Interestingly, while most of the catalytic residues were conserved across all THAP9 orthologs, D374 and D695 were only conserved across the mammalian orthologs and exhibited distinct class-specific substitutions in other classes. It is tempting to speculate that such class-specific conservation patterns of key catalytic residues, play important roles in the modification of THAP9's function

The predicted insertion domain, which lies between S415 to T604 of hTHAP9 (**Figure 11, Supplementary Table 6**), exhibited weak conservation across orthologs.

Pathogenic mutations in h*THAP9.*

We wanted to investigate the possible role of hTHAP9 in disease. No disease-specific mutation has been reported for the hTHAP9 gene (**Supplementary Table 7**). So, we examined the missense SNPs reported in the hTHAP9 gene on the Ensembl Portal[36] (which uses the 1000 Genomes project[35] data). PolyPhen-2[38] scores given on the Ensembl result table classified these SNPs into three categories: 1) score from 0 to 0.444 as "benign," 2) scores from 0.453 to 0.906 as "possibly damaging," 3) scores from 0.909 to 1 as "probably damaging."

According to Ensembl data, ~79% of missense mutations were "non-pathogenic," and ~21% of them were "pathogenic" in nature (**Table 2, Figure 12**).

Moreover, we also analyzed the missense mutations found in hTHAP9 in different cancer samples using cBioPortal[39] (**Table 3, Figure 13**). Following the Ensembl trend,~74% of missense mutations from CBioPortal were "non-pathogenic," and ~27% of them were "pathogenic" in nature. No significant hotspots for mutations in cancer were observed as the mutations were distributed throughout the THAP9 sequence.

The only missense SNP that has a global MAF > 0.05 (minor allele frequency) was rs897945 (MAF = 0.3253), making it a candidate for a derived allele (DA). Derived alleles are new alleles, having a population frequency of at least 5%, that is formed by the mutation of ancestral alleles. It has been reported that the disease-associated alleles are more likely to be low-frequency derived alleles[63]. In the *hTHAP9* gene, rs897945 yields a G → T nucleotide substitution, leading to a Leucine to Phenylalanine mutation at position 299 on Tnp_P_element (Pfam ID: PF12017) domain (**Figure 14**). This SNP may have a role in Atopy and Allergic Rhinitis in a Singapore Chinese Population[64].

THAP9 shows an altered expression in the case of Testicular & Thymic Epithelial Tumors

To investigate the gene expression profile of hTHAP9 in various cancers, we used the GEPIA[43] tool, which used cancer and matched normal from TCGA[41] and GTEx[42] portal. The results showed overexpression of hTHAP9 in testicular cancer and reduced expression in Thymic Epithelial Tumors (THYM) (**Figure 15**). We can thus speculate that hTHAP9 may have a role to play in cancers like its neighboring gene THAP9-AS1[11] and other THAP family proteins like THAP1[65] & 11[66,67]. Moreover, it is also reported that hTHAP9 shows 5-fold upregulation in TBM (Tuberculous Meningitis) patients co-infected with HIV compared to patients with TBM[68].

Discussion

Human THAP9 (hTHAP9) is a transposable element-derived gene that encodes the hTHAP9 protein, which is a homolog of Drosophila P-element transposase (DmTNP). THAP9 possesses a C2CH type DNA binding THAP domain which is shared between THAP domain-containing proteins (human THAP proteins, CDC14, CTBP1, Lin36, Lin15B, etc.), DmTNP, and zebrafish Pdre2[3,69,70]. P element-like transposable elements or P element transposase-like genes are present in other eukaryotes including the sea squirt Ciona, sea urchin, and hydra[71,72].

We observed that the orthologs of THAP9 (in 216 species) revealed remarkable conservation across species, although only 1 positively selected site was identified. Across all ortholog species we analyzed in this study, THAP9 has been subjected to a notable overall negative selection, with branch ω-values like those typically observed for housekeeping and essential genes[73]. Further supporting this notion, hTHAP9 is placed in head-2-head architecture along with the THAP9-AS1 gene[74], which is a commonly reported architecture amongst the housekeeping genes in mammals[75]. According to NCBI, in addition to the studied orthologs, THAP9 also has homologs in chimpanzees, Rhesus monkeys, dogs, cows, chickens, and frogs. In the future, it will be interesting to compare the THAP9 orthologs and homologs and also investigate the role of THAP9 in organisms that have both THAP9 homolog and ortholog sequences.

The negative selection, likely a response to strict functional constraints on THAP9, has yielded a high degree of conservation, not only at the sequence level but also at the domain organization level. Generally, proteins are more conserved at the tertiary structure level than at the amino acid sequence level[7] and random mutations and selection restrictions help in the structural and functional conservation of protein domains[77,78]. Interestingly, when comparing the THAP9 orthologs, it was observed that the zinc-coordinating C2CH motif and base-specific DNA-binding residues of the THAP domain were highly conserved. On the other hand, class-specific distinct patterns were observed in other domains. For example, certain functional residues like the catalytic D374(in hTHAP9) in the RNaseH-like domain, aligned with Glycine in all Avian orthologs. The Leucine Zipper region also had 4 more conserved Leucine other than 4 Leucine forming the L-Zipper Region. Moreover, the Leucine-Zipper, bipartite NLS, and other functional motifs present in all mammalian orthologs were absent in other classes, thus implying their possible functional importance in mammals.

We identified several disordered binding regions (DBR) in hTHAP9 protein (**Supplementary Table 1**) that are typically involved in protein-protein interactions [79]. The DBR region with the highest IUPRED[80] score is between residues 1-180 and overlaps with the THAP domain and L-Zipper region. The DBRs could also facilitate intramolecular interactions within THAP9 via motifs[81]. Moreover, predicted short linear motifs (**Supplementary Table 2**) in hTHAP9 may be involved in binding regulatory molecules like casein kinase 1 and 2 orHCF1.

The physiological role of hTHAP9 and its disease associations still remain largely unexplored. THAP9-AS1[11] (the 5' neighboring gene of THAP9) and other THAP family proteins like THAP1[65] & 11[66,67] have been implicated in various cancers. Thus, we analyzed the SNPs and cancer-associated mutations of hTHAP9 as well as its expression pattern in various cancers and observed its reduced expression in testicular cancer (**Figure. 15**). It is interesting to note that transposition of P-element, the well-studied homolog of hTHAP9, causes hybrid dysgenesis leading to male sterility in Drosophila[82].

References

1. Su, W., Zuo, T. & Peterson, T. Ectopic Expression of a Maize Gene Is Induced by Composite Insertions Generated Through Alternative Transposition. *Genetics* **216**, 1039–1049 (2020).
2. Bourque, G. *et al.* Ten things you should know about transposable elements. *Genome Biol.* **19**, 199 (2018).
3. Majumdar, S. & Rio, D. C. P transposable elements in Drosophila and other eukaryotic organisms. *Microbiol. Spectr.* **3**, MDNA3-0004–2014 (2015).
4. Sabogal, A., Lyubimov, A. Y., Corn, J. E., Berger, J. M. & Rio, D. C. THAP proteins target specific DNA sites through bipartite recognition of adjacent major and minor grooves. *Nat. Struct. Mol. Biol.* **17**, 117–123 (2010).
5. Campagne, S., Saurel, O., Gervais, V. & Milon, A. Structural determinants of specific DNA-recognition by the THAP zinc finger. *Nucleic Acids Res.* **38**, 3466–3476 (2010).
6. Richter, A. *et al.* In-depth Characterization of the Homodimerization Domain of the Transcription Factor THAP1 and Dystonia-Causing Mutations Therein. *J. Mol. Neurosci.* **62**, 11–16 (2017).
7. Balakrishnan, M. P. *et al.* THAP5 is a human cardiac-specific inhibitor of cell cycle that is cleaved by the proapoptotic Omi/HtrA2 protease during cell death. *Am. J. Physiol. Heart*

Circ. Physiol. **297**, H643-653 (2009).

8. Leite, K. R. M. *et al.* MicroRNA 100: a context dependent miRNA in prostate cancer. *Clinics* **68**, 797–802 (2013).
9. De Souza Santos, E., De Bessa, S. A., Netto, M. M. & Nagai, M. A. Silencing of LRRC49 and THAP10 genes by bidirectional promoter hypermethylation is a frequent event in breast cancer. *Int. J. Oncol.* **33**, 25–31 (2008).
10. Parker, J. B., Palchaudhuri, S., Yin, H., Wei, J. & Chakravarti, D. A transcriptional regulatory role of the THAP11-HCF-1 complex in colon cancer cell function. *Mol. Cell. Biol.* **32**, 1654–1670 (2012).
11. Li, N. *et al.* lncRNA THAP9-AS1 Promotes Pancreatic Ductal Adenocarcinoma Growth and Leads to a Poor Clinical Outcome via Sponging miR-484 and Interacting with YAP. *Clin. Cancer Res. Off. J. Am. Assoc. Cancer Res.* **26**, 1736–1748 (2020).
12. Nielsen, R., Hellmann, I., Hubisz, M., Bustamante, C. & Clark, A. G. Recent and ongoing selection in the human genome. *Nat. Rev. Genet.* **8**, 857–868 (2007).
13. Thompson, J. D., Higgins, D. G. & Gibson, T. J. CLUSTAL W: improving the sensitivity of progressive multiple sequence alignment through sequence weighting, position-specific gap penalties and weight matrix choice. *Nucleic Acids Res.* **22**, 4673–4680 (1994).
14. Kumar, S., Stecher, G., Li, M., Knyaz, C. & Tamura, K. MEGA X: Molecular Evolutionary Genetics Analysis across Computing Platforms. *Mol. Biol. Evol.* **35**, 1547–1549 (2018).
15. Kumar, S., Stecher, G., Suleski, M. & Hedges, S. B. TimeTree: A Resource for Timelines, Timetrees, and Divergence Times. *Mol. Biol. Evol.* **34**, 1812–1819 (2017).
16. Suyama, M., Torrents, D. & Bork, P. PAL2NAL: robust conversion of protein sequence alignments into the corresponding codon alignments. *Nucleic Acids Res.* **34**, W609-612 (2006).
17. Letunic, I. & Bork, P. Interactive Tree Of Life (iTOL) v4: recent updates and new developments. *Nucleic Acids Res.* **47**, W256–W259 (2019).

18. Pond, S. L. K., Poon, A. F. Y. & Frost, S. D. W. Estimating selection pressures on alignments of coding sequences. in *The Phylogenetic Handbook* (eds. Lemey, P., Salemi, M. & Vandamme, A.-M.) 419–490 (Cambridge University Press, 2009). doi:10.1017/CBO9780511819049.016.
19. Afgan, E. *et al.* The Galaxy platform for accessible, reproducible and collaborative biomedical analyses: 2016 update. *Nucleic Acids Res.* **44**, W3–W10 (2016).
20. Yang, Z. PAML: a program package for phylogenetic analysis by maximum likelihood. *Comput. Appl. Biosci. CABIOS* **13**, 555–556 (1997).
21. Price, M. N., Dehal, P. S. & Arkin, A. P. FastTree 2--approximately maximum-likelihood trees for large alignments. *PloS One* **5**, e9490 (2010).
22. Kosakovsky Pond, S. L. & Frost, S. D. W. Not so different after all: a comparison of methods for detecting amino acid sites under selection. *Mol. Biol. Evol.* **22**, 1208–1222 (2005).
23. Murrell, B. *et al.* FUBAR: a fast, unconstrained bayesian approximation for inferring selection. *Mol. Biol. Evol.* **30**, 1196–1205 (2013).
24. Murrell, B. *et al.* Detecting individual sites subject to episodic diversifying selection. *PLoS Genet.* **8**, e1002764 (2012).
25. Spielman, S. J. *et al.* Evolution of Viral Genomes: Interplay Between Selection, Recombination, and Other Forces. *Methods Mol. Biol. Clifton NJ* **1910**, 427–468 (2019).
26. Letunic, I., Khedkar, S. & Bork, P. SMART: recent updates, new developments and status in 2020. *Nucleic Acids Res.* **49**, D458–D460 (2021).
27. El-Gebali, S. *et al.* The Pfam protein families database in 2019. *Nucleic Acids Res.* **47**, D427–D432 (2019).
28. Kumar, M. *et al.* ELM-the eukaryotic linear motif resource in 2020. *Nucleic Acids Res.* **48**, D296–D306 (2020).
29. Bailey, T. L. *et al.* MEME SUITE: tools for motif discovery and searching. *Nucleic Acids Res.* **37**, W202-208 (2009).

30. de Castro, E. *et al.* ScanProsite: detection of PROSITE signature matches and ProRule-associated functional and structural residues in proteins. *Nucleic Acids Res.* **34**, W362-365 (2006).
31. Ward, J. J., Sodhi, J. S., McGuffin, L. J., Buxton, B. F. & Jones, D. T. Prediction and functional analysis of native disorder in proteins from the three kingdoms of life. *J. Mol. Biol.* **337**, 635–645 (2004).
32. Buchan, D. W. A. & Jones, D. T. The PSIPRED Protein Analysis Workbench: 20 years on. *Nucleic Acids Res.* **47**, W402–W407 (2019).
33. Wilkins, M. R. *et al.* Protein identification and analysis tools in the ExPASy server. *Methods Mol. Biol. Clifton NJ* **112**, 531–552 (1999).
34. Rice, P., Longden, I. & Bleasby, A. EMBOSS: the European Molecular Biology Open Software Suite. *Trends Genet. TIG* **16**, 276–277 (2000).
35. Clarke, L. *et al.* The 1000 Genomes Project: data management and community access. *Nat. Methods* **9**, 459–462 (2012).
36. Howe, K. L. *et al.* Ensembl 2021. *Nucleic Acids Res.* **49**, D884–D891 (2021).
37. Adzhubei, I. A. *et al.* A method and server for predicting damaging missense mutations. *Nat. Methods* **7**, 248–249 (2010).
38. Adzhubei, I., Jordan, D. M. & Sunyaev, S. R. Predicting Functional Effect of Human Missense Mutations Using PolyPhen-2. *Curr. Protoc. Hum. Genet.* **76**, 7.20.1-7.20.41 (2013).
39. Cerami, E. *et al.* The cBio Cancer Genomics Portal: An Open Platform for Exploring Multidimensional Cancer Genomics Data. *Cancer Discov.* **2**, 401–404 (2012).
40. McLaren, W. *et al.* The Ensembl Variant Effect Predictor. *Genome Biol.* **17**, 122 (2016).
41. Tomczak, K., Czerwińska, P. & Wiznerowicz, M. The Cancer Genome Atlas (TCGA): an immeasurable source of knowledge. *Contemp. Oncol.* **19**, A68–A77 (2015).
42. GTEx Consortium. The Genotype-Tissue Expression (GTEx) project. *Nat. Genet.* **45**,

580–585 (2013).

43. Tang, Z. *et al.* GEPIA: a web server for cancer and normal gene expression profiling and interactive analyses. *Nucleic Acids Res.* **45**, W98–W102 (2017).
44. Majumdar, S., Singh, A. & Rio, D. C. The Human THAP9 Gene Encodes an Active P-Element DNA Transposase. *Science* **339**, 446–448 (2013).
45. Hall, B. G. Building phylogenetic trees from molecular data with MEGA. *Mol. Biol. Evol.* **30**, 1229–1235 (2013).
46. Chu, D. & Wei, L. Nonsynonymous, synonymous and nonsense mutations in human cancer-related genes undergo stronger purifying selections than expectation. *BMC Cancer* **19**, 359 (2019).
47. Kryazhimskiy, S. & Plotkin, J. B. The Population Genetics of dN/dS. *PLOS Genet.* **4**, e1000304 (2008).
48. Sanghavi, H. M. & Majumdar, S. Oligomerization of THAP9 Transposase via Amino-Terminal Domains. *Biochemistry* **60**, 1822–1835 (2021).
49. Udenwobele, D. I. *et al.* Myristoylation: An Important Protein Modification in the Immune Response. *Front. Immunol.* **8**, 751 (2017).
50. Robbins, J., Dilwortht, S. M., Laskey, R. A. & Dingwall, C. Two interdependent basic domains in nucleoplasmin nuclear targeting sequence: Identification of a class of bipartite nuclear targeting sequence. *Cell* **64**, 615–623 (1991).
51. Sheldon, L. A. & Kingston, R. E. Hydrophobic coiled-coil domains regulate the subcellular localization of human heat shock factor 2. *Genes Dev.* **7**, 1549–1558 (1993).
52. Nagoshi, E., Imamoto, N., Sato, R. & Yoneda, Y. Nuclear Import of Sterol Regulatory Element–binding Protein-2, a Basic Helix-Loop-Helix–Leucine Zipper (bHLH-Zip)–containing Transcription Factor, Occurs through the Direct Interaction of Importin β with HLH-Zip. *Mol. Biol. Cell* **10**, 2221–2233 (1999).
53. Chu, E. C. & Tarnawski, A. S. PTEN regulatory functions in tumor suppression and cell

biology. *Med. Sci. Monit. Int. Med. J. Exp. Clin. Res.* **10**, RA235-241 (2004).

54. The UniProt Consortium. UniProt: a worldwide hub of protein knowledge. *Nucleic Acids Res.* **47**, D506–D515 (2019).
55. Sharma, V., Thakore, P. & Majumdar, S. THAP9 Transposase Cleaves DNA via Conserved Acidic Residues in an RNaseH-Like Domain. *Cells* **10**, 1351 (2021).
56. Sanghavi, H. M., Mallajosyula, S. S. & Majumdar, S. Classification of the human THAP protein family identifies an evolutionarily conserved coiled coil region. *BMC Struct. Biol.* **19**, 4 (2019).
57. Ghanim, G. E., Kellogg, E. H., Nogales, E. & Rio, D. C. Structure of a P element transposase-DNA complex reveals unusual DNA structures and GTP-DNA contacts. *Nat. Struct. Mol. Biol.* **26**, 1013–1022 (2019).
58. Haren, L., Polard, P., Ton-Hoang, B. & Chandler, M. Multiple oligomerisation domains in the IS911 transposase: a leucine zipper motif is essential for activity. *J. Mol. Biol.* **283**, 29–41 (1998).
59. Lee, C. C., Mul, Y. M. & Rio, D. C. The Drosophila P-element KP repressor protein dimerizes and interacts with multiple sites on P-element DNA. *Mol. Cell. Biol.* **16**, 5616–5622 (1996).
60. Hickman, A. B., Chandler, M. & Dyda, F. Integrating prokaryotes and eukaryotes: DNA transposases in light of structure. *Crit. Rev. Biochem. Mol. Biol.* **45**, 50–69 (2010).
61. Nesmelova, I. V. & Hackett, P. B. DDE transposases: Structural similarity and diversity. *Adv. Drug Deliv. Rev.* **62**, 1187–1195 (2010).
62. Hickman, A. B. & Dyda, F. DNA Transposition at Work. *Chem. Rev.* **116**, 12758–12784 (2016).
63. Lachance, J. Disease-associated alleles in genome-wide association studies are enriched for derived low frequency alleles relative to HapMap and neutral expectations. *BMC Med. Genomics* **3**, 57 (2010).

64. Andiappan, A. K. *et al.* Genome-Wide Association Study for Atopy and Allergic Rhinitis in a Singapore Chinese Population. *PLOS ONE* **6**, e19719 (2011).

65. Roussigne, M., Cayrol, C., Clouaire, T., Amalric, F. & Girard, J.-P. THAP1 is a nuclear proapoptotic factor that links prostate-apoptosis-response-4 (Par-4) to PML nuclear bodies. *Oncogene* **22**, 2432–2442 (2003).

66. Zhang, J. *et al.* THAP11 Functions as a Tumor Suppressor in Gastric Cancer through Regulating c-Myc Signaling Pathways. *BioMed Res. Int.* **2020**, e7838924 (2020).

67. Parker, J. B., Palchaudhuri, S., Yin, H., Wei, J. & Chakravarti, D. A Transcriptional Regulatory Role of the THAP11–HCF-1 Complex in Colon Cancer Cell Function. *Mol. Cell. Biol.* **32**, 1654–1670 (2012).

68. Kumar, G. S. S. *et al.* Gene Expression Profiling of Tuberculous Meningitis Co-infected with HIV. *J. Proteomics Bioinform.* **5**, 235–244 (2012).

69. Hammer, S. E., Strehl, S. & Hagemann, S. Homologs of Drosophila P transposons were mobile in zebrafish but have been domesticated in a common ancestor of chicken and human. *Mol. Biol. Evol.* **22**, 833–844 (2005).

70. Hagemann, S. & Hammer, S. E. The implications of DNA transposons in the evolution of P elements in zebrafish (Danio rerio). *Genomics* **88**, 572–579 (2006).

71. Kimbacher, S., Gerstl, I., Velimirov, B. & Hagemann, S. Drosophila P transposons of the urochordata Ciona intestinalis. *Mol. Genet. Genomics MGG* **282**, 165–172 (2009).

72. Chapman, J. A. *et al.* The dynamic genome of Hydra. *Nature* **464**, 592–596 (2010).

73. Lv, W. *et al.* Comparing the evolutionary conservation between human essential genes, human orthologs of mouse essential genes and human housekeeping genes. *Brief. Bioinform.* **16**, 922–931 (2015).

74. Sharma, V., Thakore, P., Krishnan, M. & Majumdar, S. *Stress induced Differential Expression of THAP9 & THAP9-AS1 in the S-phase of cell cycle*. 2021.02.11.430738 https://www.biorxiv.org/content/10.1101/2021.02.11.430738v1 (2021)

doi:10.1101/2021.02.11.430738.

75. Adachi, N. & Lieber, M. R. Bidirectional Gene Organization: A Common Architectural Feature of the Human Genome. *Cell* **109**, 807–809 (2002).
76. Grishin, N. V. Fold change in evolution of protein structures. *J. Struct. Biol.* **134**, 167–185 (2001).
77. Bagowski, C. P., Bruins, W. & Te Velthuis, A. J. W. The nature of protein domain evolution: shaping the interaction network. *Curr. Genomics* **11**, 368–376 (2010).
78. Ponting, C. P. & Russell, R. R. The natural history of protein domains. *Annu. Rev. Biophys. Biomol. Struct.* **31**, 45–71 (2002).
79. Mészáros, B., Dosztányi, Z. & Simon, I. Disordered binding regions and linear motifs--bridging the gap between two models of molecular recognition. *PloS One* **7**, e46829 (2012).
80. Dosztányi, Z. Prediction of protein disorder based on IUPred. *Protein Sci. Publ. Protein Soc.* **27**, 331–340 (2018).
81. Stein, A., Pache, R. A., Bernadó, P., Pons, M. & Aloy, P. Dynamic interactions of proteins in complex networks: a more structured view. *FEBS J.* **276**, 5390–5405 (2009).
82. Kidwell, M. G. Evolution of hybrid dysgenesis determinants in Drosophila melanogaster. *Proc. Natl. Acad. Sci. U. S. A.* **80**, 1655–1659 (1983).

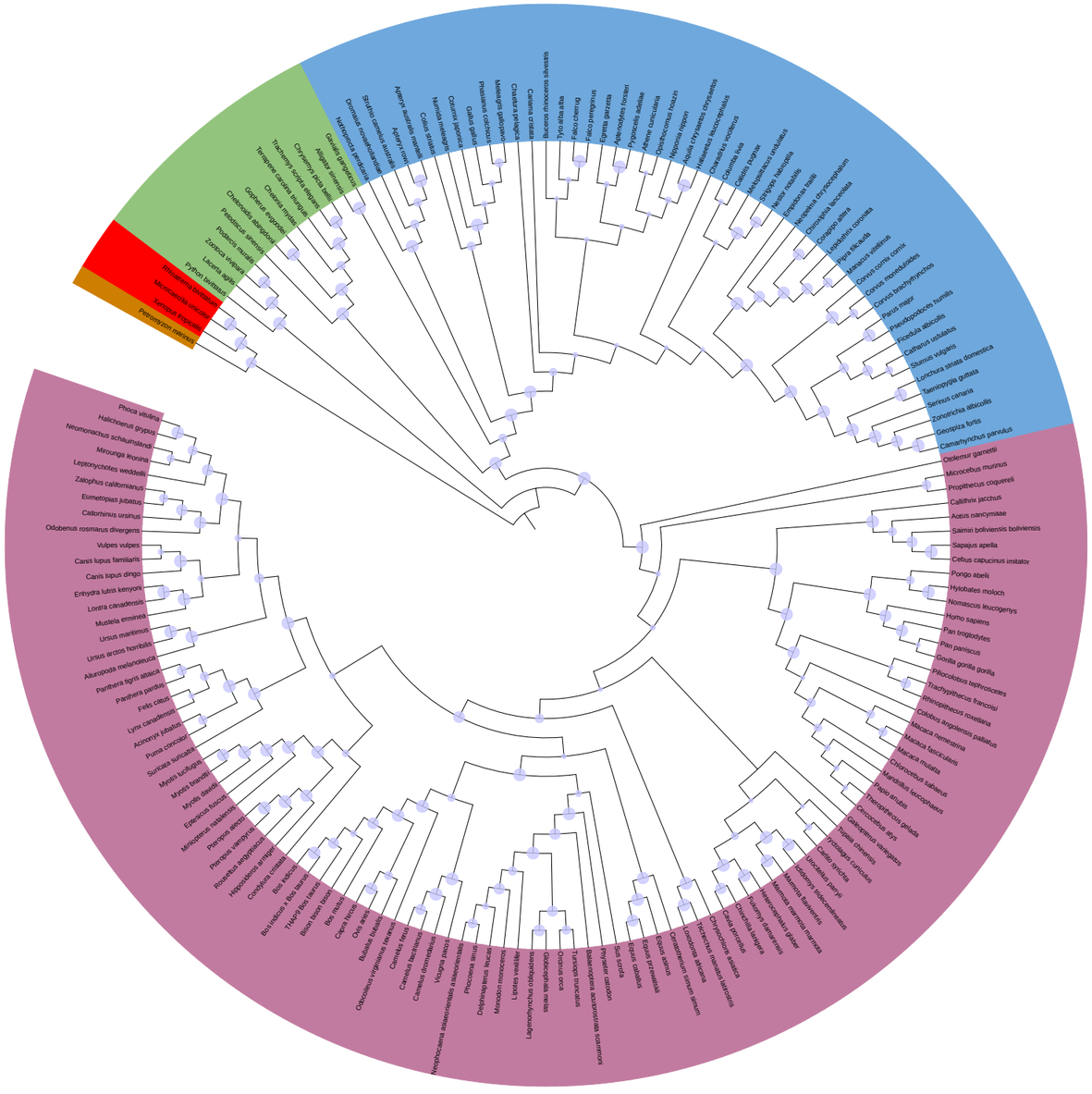
Colored ranges
Amphibia
Hyperoartia
Reptilia
Aves
Mammalia
bootstrap
0
0.25
0.5
0.75
1

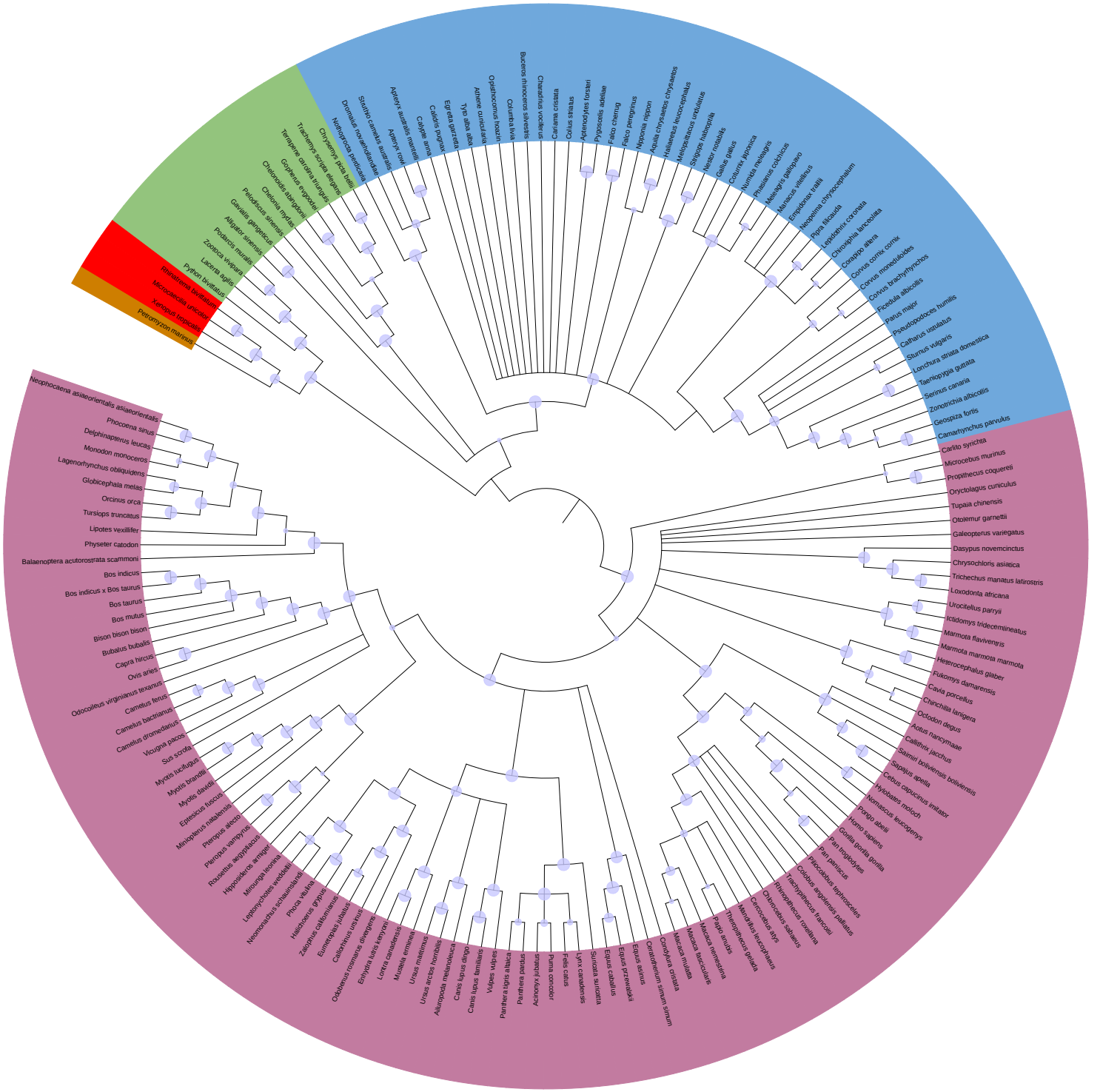
Colored ranges
Amphibia
Hyperoartia
Reptilia
Aves
Mammalia
bootstrap
0.52
0.64
0.76
0.88
1
Petromyzon marinus
Xenopus tropicalis
Microcaudella uniscalata
Rhinastrema bivittatum
Python bivittatus
Lacerta agilis
Zootoca vivipara
Alligator sinensis
Gavialis gangeticus
Podarcis muralis
Pelodiscus sinensis
Chelonia mydas
Chelonoidis abingdonii
Gopherus evgoodei
Terrapene carolina triunguis
Trachemys scripta elegans
Chrysemys picta bellii
Notophoxus neglectus
Dromaius novaehollandiae
Struthio camelus australis
Apteryx rowi
Apteryx australis mantelli
Calypte anna
Caloris pupnus
Egretta garzetta
Tyto alba alba
Anhima cornuta
Opisthocomus hoazin
Columba livia
Buceros rhinoceros silvestris
Chaetura vocifer
Cariama cristata
Colius striatus
Aptenodytes forsteri
Pygoscelis adeliae
Falco cherrug
Falco peregrinus
Nyctonia nippon
Aquila chrysaetos chrysaetos
Haliaeetus leucocephalus
Melopsittacus undulatus
Bulbigoje haldeprilla
Nestor notabilis
Gallus gallus
Coturnix japonica
Numida meleagris
Phasianus colchicus
Meleagris gallopavo
Monacus vitellinus
Empidonax traillii
Neopelma chrysocephalum
Pipra filicauda
Lepidotinix coronata
Chiroxiphia lanceolata
Corapipo altera
Corvus corax corax
Corvus monedulides
Corvus brachyrhynchos
Ficedula albicollis
Parus major
Pseudopodoces humilis
Cathartus usiulatus
Sturnus vulgaris
Lonchura striata domestica
Taeniopygia guttata
Serinus canaria
Zonotrichia albicollis
Geostiza fortis
Camarhynchus parvulus
Carlito syrichta
Microcebus murinus
Propithecus coquereii
Oryctolagus cuniculus
Tupaia chinensis
Otolemur garnettii
Galeopterus variegatus
Dasypus novemcinctus
Chrysochloris asiatica
Trichechus manatus latirostris
Loxodonta africana
Urocitellus parryii
Ictidomys tridecemlineatus
Marmota flaviventris
Marmota marmota marmota
Heterocephalus glaber
Fukomys damarensis
Cavia porcellus
Chinchilla lanigera
Octodon degus
Aotus nancymaae
Callithrix jacchus
Saimiri boliviensis boliviensis
Sapajus apella
Cebus capucinus imitator
Hylobates moloch
Nomascus leucogenys
Pongo abelii
Homo sapiens
Gorilla gorilla gorilla
Pan troglodytes
Pan paniscus
Colobus angolensis palliatus
Piliocolobus tephrosceles
Trachypithecus francoisi
Rhinopithecus roxellana
Chlorocebus sabaeus
Cercocebus atys
Macaca fascicularis
Macaca nemestrina
Papio anubis
Theropithecus gelada
Mandrillus leucophaeus
Macaca mulatta
Cercopithecus nigroviridis
Cercopithecus ascanius
Cercopithecus mitis
Cercopithecus neglectus
Chlorocebus pygerythrus
Erythrocebus patas
Colobus guereza
Colobus angolensis sharicus
Colobus satanas
Colobus vellerosus
Colobus polykomos
Colobus leucomeris
Colobus tephrosceles
Colobus angolensis palliatus
Colobus angolensis ruficrus
Colobus angolensis cottoni
Colobus angolensis sharicus

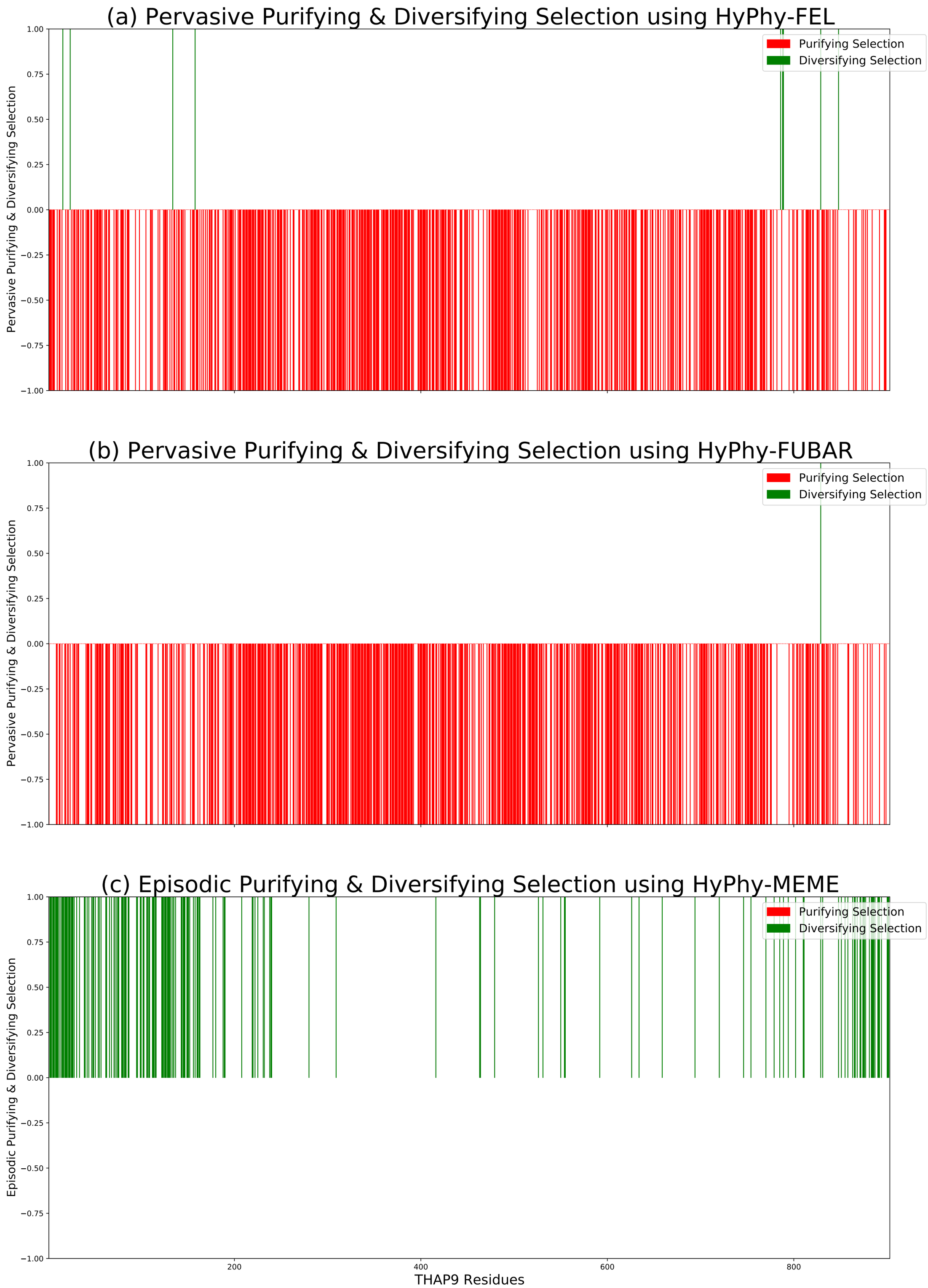
(a) Pervasive Purifying & Diversifying Selection using HyPhy-FEL
Pervasive Purifying & Diversifying Selection
Purifying Selection
Diversifying Selection
(b) Pervasive Purifying & Diversifying Selection using HyPhy-FUBAR
Pervasive Purifying & Diversifying Selection
Purifying Selection
Diversifying Selection
(c) Episodic Purifying & Diversifying Selection using HyPhy-MEME
Episodic Purifying & Diversifying Selection
Purifying Selection
Diversifying Selection
1.00
0.75
0.50
0.25
0.00
−0.25
−0.50
−0.75
−1.00
200
400
600
800
THAP9 Residues

Amino Acid Composition of hTHAP9

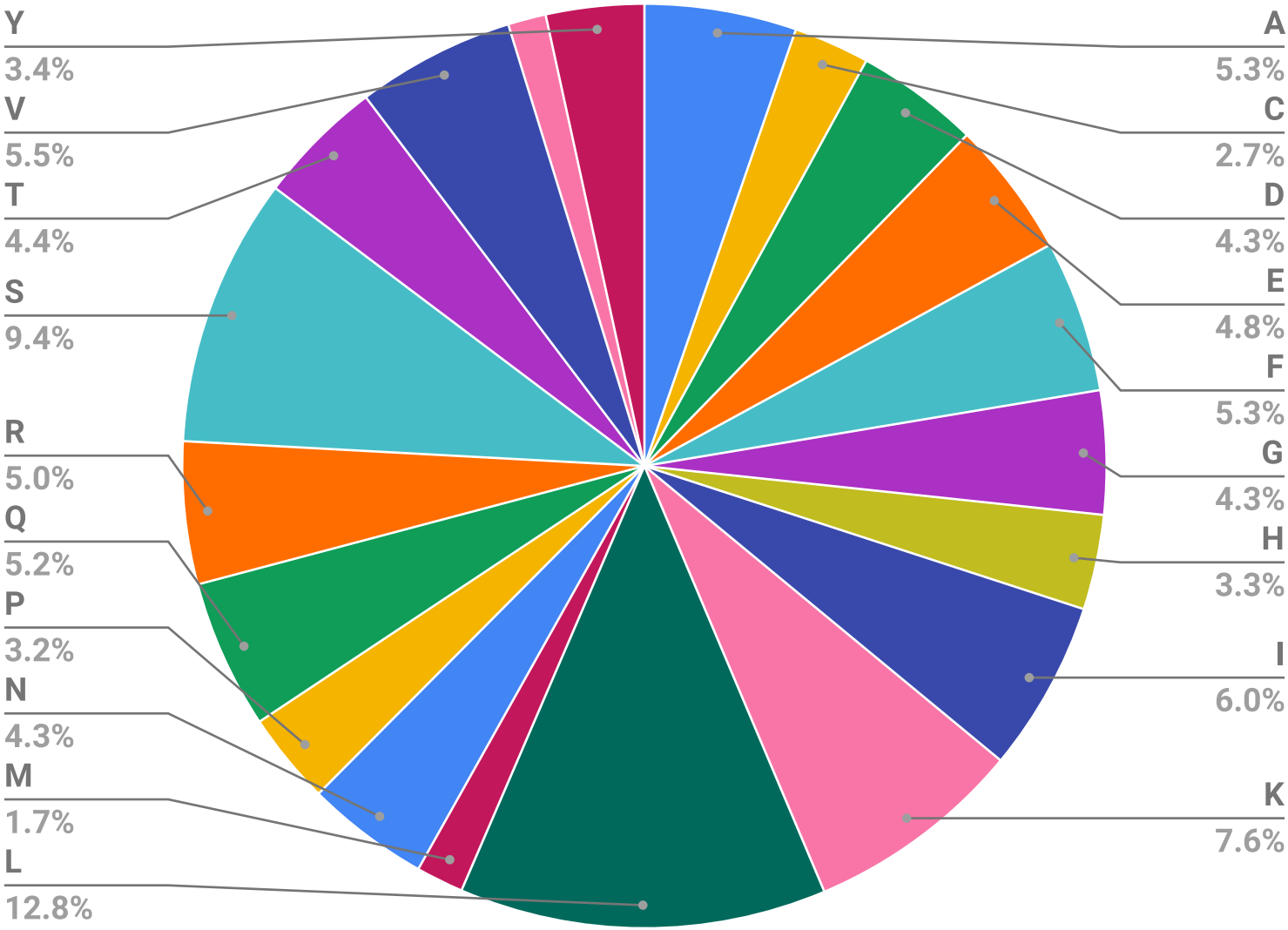

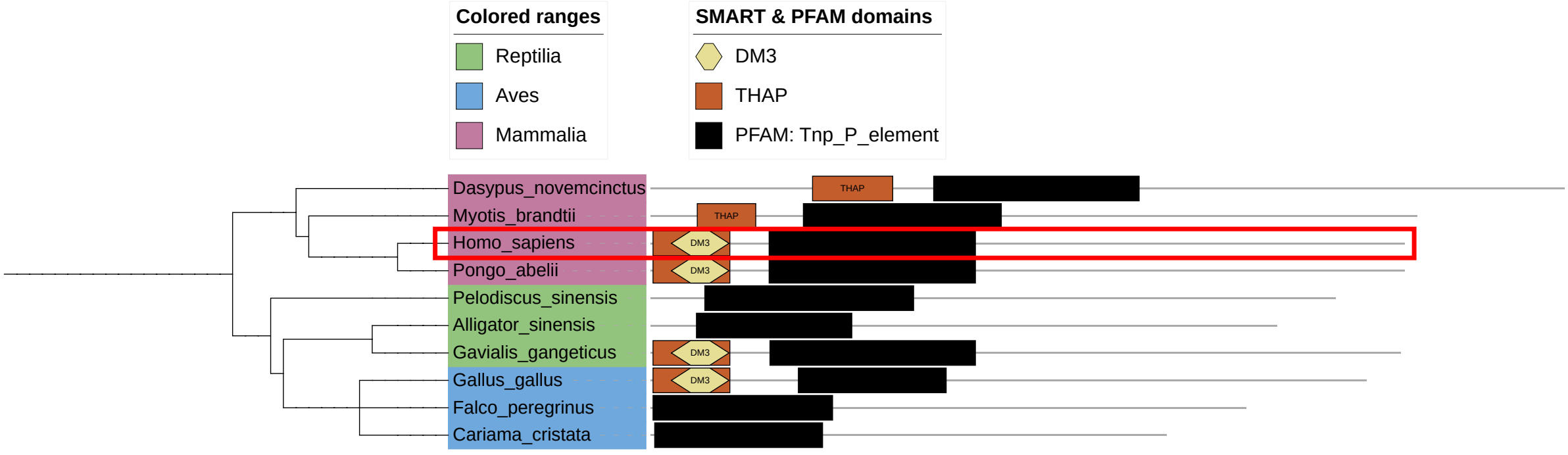
Colored ranges
Reptilia
Aves
Mammalia
SMART & PFAM domains
DM3
THAP
PFAM: Tnp_P_element
Dasypus_novemcinctus
Myotis_brandtii
Homo_sapiens
Pongo_abelii
Pelodiscus_sinensis
Alligator_sinensis
Gavialis_gangeticus
Gallus_gallus
Falco_peregrinus
Cariama_cristata
THAP
THAP
DM3
DM3
DM3
DM3

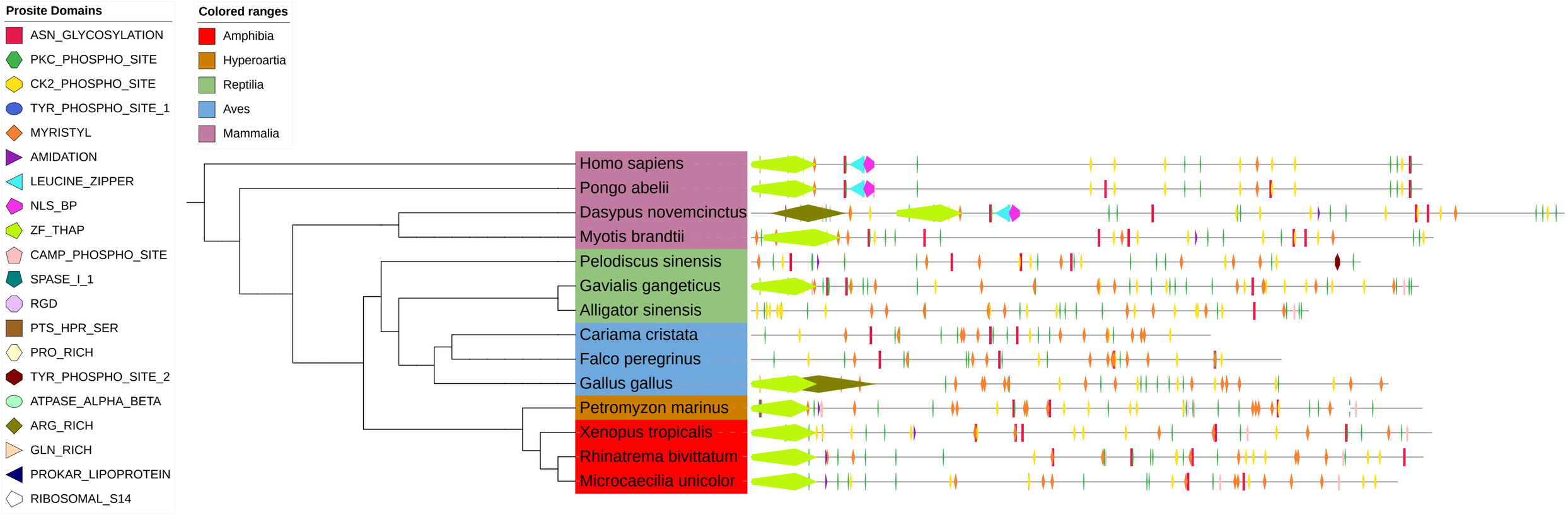
Prosite Domains
ASN_GLYCOSYLATION
PKC_PHOSPHO_SITE
CK2_PHOSPHO_SITE
TYR_PHOSPHO_SITE_1
MYRISTYL
AMIDATION
LEUCINE_ZIPPER
NLS_BP
ZF_THAP
CAMP_PHOSPHO_SITE
SPASE_I_1
RGD
PTS_HPR_SER
PRO_RICH
TYR_PHOSPHO_SITE_2
ATPASE_ALPHA_BETA
ARG_RICH
GLN_RICH
PROKAR_LIPOPROTEIN
RIBOSOMAL_S14
Colored ranges
Amphibia
Hyperoartia
Reptilia
Aves
Mammalia
Homo sapiens
Pongo abelii
Dasypus novemcinctus
Myotis brandtii
Pelodiscus sinensis
Gavialis gangeticus
Alligator sinensis
Cariama cristata
Falco peregrinus
Gallus gallus
Petromyzon marinus
Xenopus tropicalis
Rhinatrema bivittatum
Microcaecilia unicolor

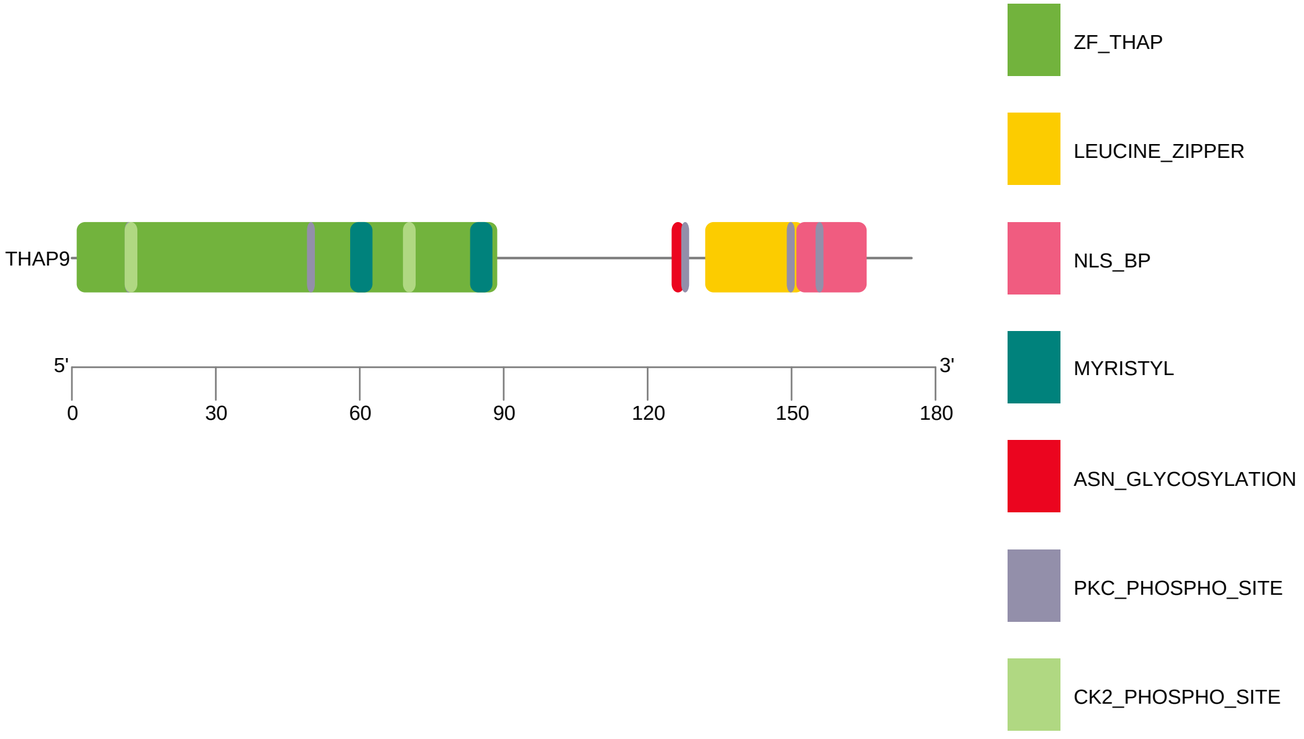
THAP9
5'
3'
0
30
60
90
120
150
180
ZF_THAP
LEUCINE_ZIPPER
NLS_BP
MYRISTYL
ASN_GLYCOSYLATION
PKC_PHOSPHO_SITE
CK2_PHOSPHO_SITE

Colored ranges

- Amphibia
- Hyperoartia
- Reptilia
- Aves
- Mammalia

bootstrap

- 0
- 0.25
- 0.5
- 0.75
- 1

Motifs

- GITVLAVTSDATAHSVZMAKALGIHIDGDNMKCTFQHPSSSSQQIAYFFD
- WDPSSHHLQGFMDFGLGKLDADETPLASETILLMAVGISGHWRTPLGYFF
- KWELYNWRETAEYSTEMKQFACTLYLCSSKVYDYVRKILKLPHSSILRTW
- FHQFPTDTIQRSKWIRAVNRVDPRSKKIWIPGPGAILCSKHFQESDFESY
- EAKTIFVTLSDTSNNQIIKGKRKLGFLGFLLNAESLKWLYQNY
- PPFQNCIGTIHFLRLINNLFDIFNSRNCYGKGLKGPLLPETYSKINHVLI
- SCHLLRLIRNAFQNFQSIQFJNGTAHWQHLVELVALEEQEL
- CKPSPGFNSNIFSFLQRRVENGDQLYQYCSLIIKGISLKQQ
- FVDLDEHLFDGEVCAINHFVKLLKDIIICFLNI
- PKVMPFPYLLTYKFSQDHLELFLKMLRQV
- TCEDCISALYASDLKASKIGSLLCVKKKNGLHFPSESLCRVINICERVVR
- MERIPRKLANLKNHVLKVNCAAQLFSESVASALE
- GVHLKGKARQKILKQPLPDNSQEVATEDHNYSLKRPLTI
- SVKNYRMIKKRKGLRLIDALVEEKLLSE
- WTVQRQYGVSVIKTLFHKEDICQDWSBCS
- VTSSNPTCMAFQKAYHNLETRY
- LSEALLDLSDHRRNLTCCAGYVANKLSAL
- MTRSCSAVGCSTRDTVLSRER
- VNRASGYLQAQLLRLTIGKLS
- GIRRKLKKGAVPSVSLYKVPQ
- KQRELYLZQKILCELS
- VFLSEVSILDISIARRTDLAL
- AEKLAEVQQMLQVSK
- WSSLQDYKCSSFANT
- KHHSERTEMKTLSRK
- ECLLRAQFSDF
- NKFRHLLSNDGYPFK
- THSRMAVYELL
- GSIRAQYNPARGRTLATEYPY
- RAKDVAQY

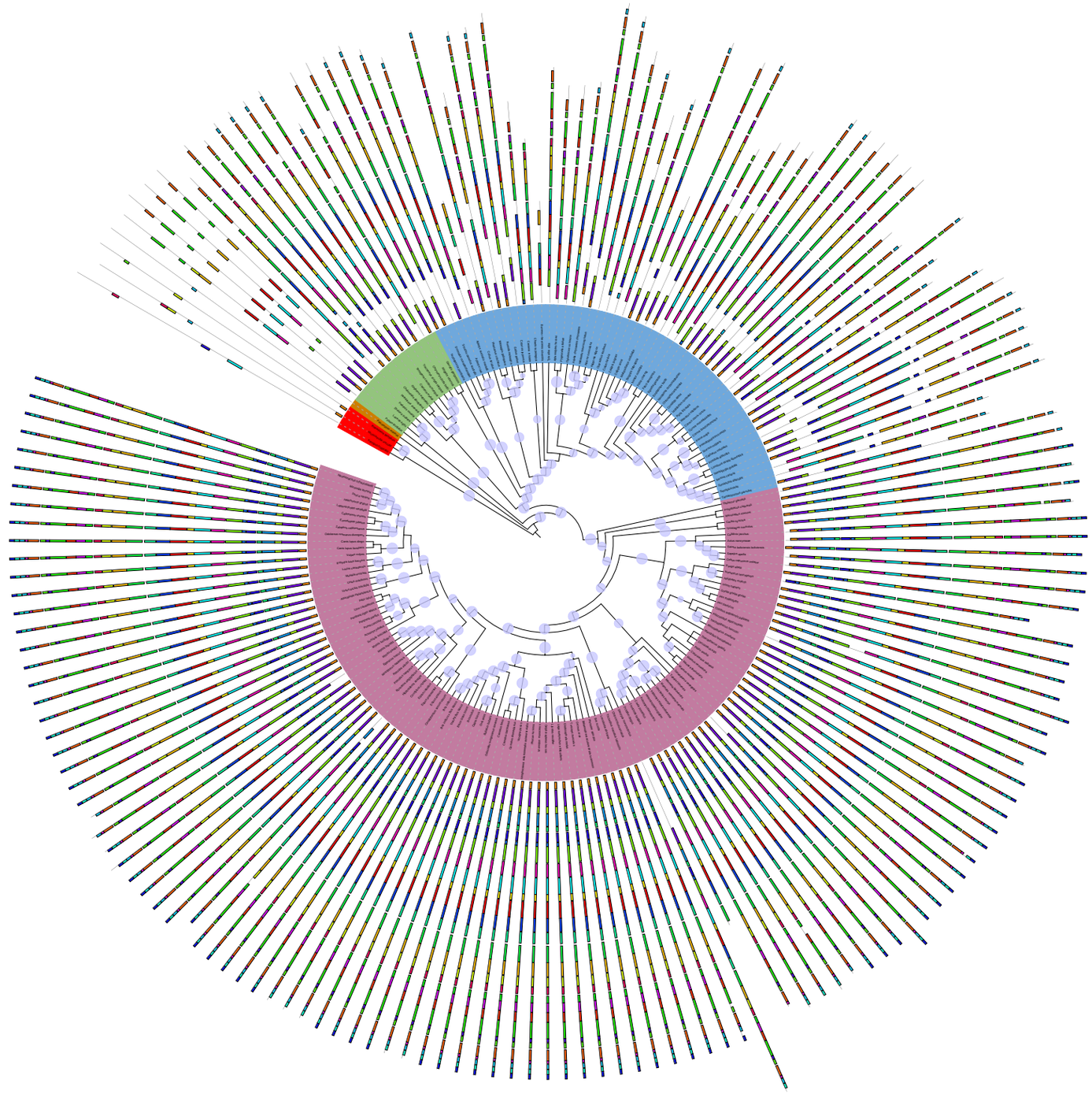

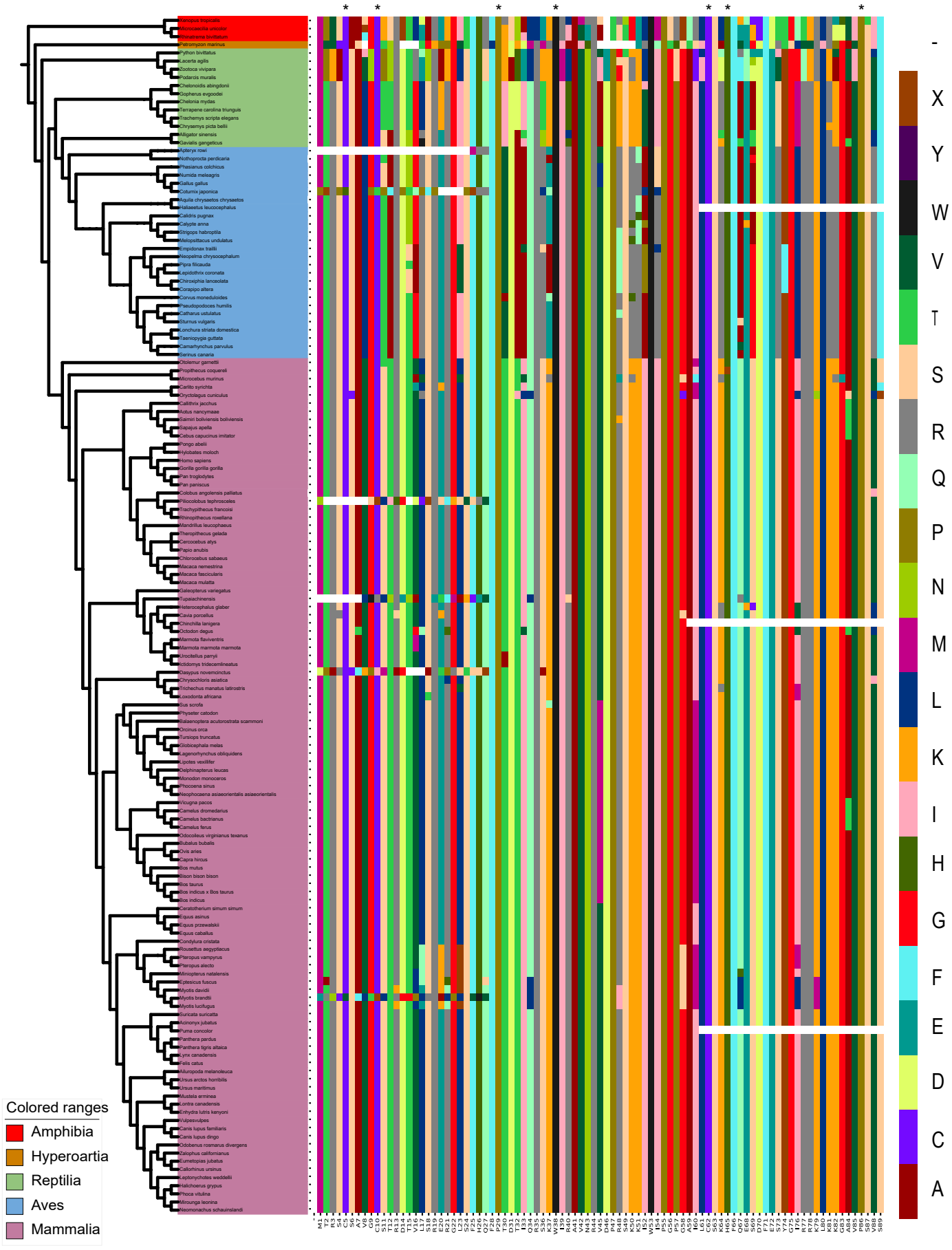
Xenopus tropicalis
Microcaecilia unicolor
Rhinatrema bivittatum
Petromyzon marinus
Python bivittatus
Lacerta agilis
Zootoca vivipara
Podarcis muralis
Chelonoidis abingdonii
Gopherus evgoodei
Chelonia mydas
Terrapene carolina triunguis
Trachemys scripta elegans
Chrysemys picta bellii
Alligator sinensis
Gavialis gangeticus
Apteryx rowi
Nothoprocta perdicaria
Phasianus colchicus
Numida meleagris
Gallus gallus
Coturnix japonica
Aquila chrysaetos chrysaetos
Haliaeetus leucocephalus
Calidris pugnax
Calypte anna
Strigops habroptila
Melopsittacus undulatus
Empidonax traillii
Neopelma chrysocephalum
Pipra filicauda
Lepidothrix coronata
Chiroxiphia lanceolata
Corapipo altera
Corvus moneduloides
Pseudopodoces humilis
Catharus ustulatus
Sturnus vulgaris
Lonchura striata domestica
Taeniopygia guttata
Camarhynchus parvulus
Serinus canaria
Otolemur garnettii
Propithecus coquereli
Microcebus murinus
Carlito syrichta
Oryctolagus cuniculus
Callithrix jacchus
Aotus nancymaae
Saimiri boliviensis boliviensis
Sapajus apella
Cebus capucinus imitator
Pongo abelii
Hylobates moloch
Homo sapiens
Gorilla gorilla gorilla
Pan troglodytes
Pan paniscus
Colobus angolensis palliatus
Piliocolobus tephrosceles
Trachypithecus francoisi
Rhinopithecus roxellana
Mandrillus leucophaeus
Theropithecus gelada
Cercocebus atys
Papio anubis
Chlorocebus sabaeus
Macaca nemestrina
Macaca fascicularis
Macaca mulatta
Galeopterus variegatus
Tupaiachinensis
Heterocephalus glaber
Cavia porcellus
Chinchilla lanigera
Octodon degus
Marmota flaviventris
Marmota marmota marmota
Urocitellus parryii
Ictidomys tridecemlineatus
Dasypus novemcinctus
Chrysochloris asiatica
Trichechus manatus latirostris
Loxodonta africana
Sus scrofa
Physeter catodon
Balaenoptera acutorostrata scammoni
Orcinus orca
Tursiops truncatus
Globicephala melas
Lagenorhynchus obliquidens
Lipotes vexillifer
Delphinapterus leucas
Monodon monoceros
Phocoena sinus
Neophocaena asiaeorientalis asiaeorientalis
Vicugna pacos
Camelus dromedarius
Camelus bactrianus
Camelus ferus
Odocoileus virginianus texanus
Bubalus bubalis
Ovis aries
Capra hircus
Bos mutus
Bison bison bison
Bos taurus
Bos indicus x Bos taurus
Bos indicus
Ceratotherium simum simum
Equus asinus
Equus przewalskii
Equus caballus
Condylura cristata
Rousettus aegyptiacus
Pteropus vampyrus
Pteropus alecto
Miniopterus natalensis
Eptesicus fuscus
Myotis davidii
Myotis brandtii
Myotis lucifugus
Suricata suricatta
Acinonyx jubatus
Puma concolor
Panthera pardus
Panthera tigris altaica
Lynx canadensis
Felis catus
Ailuropoda melanoleuca
Ursus arctos horribilis
Ursus maritimus
Mustela erminea
Lontra canadensis
Enhydra lutris kenyoni
Vulpesvulpes
Canis lupus familiaris
Canis lupus dingo
Odobenus rosmarus divergens
Zalophus californianus
Eumetopias jubatus
Callorhinus ursinus
Leptonychotes weddellii
Halichoerus grypus
Phoca vitulina
Mirounga leonina
Neomonachus schauinslandi
Colored ranges
Amphibia
Hyperoartia
Reptilia
Aves
Mammalia
-
X
Y
W
V
T
S
R
Q
P
N
M
L
K
I
H
G
F
E
D
C
A

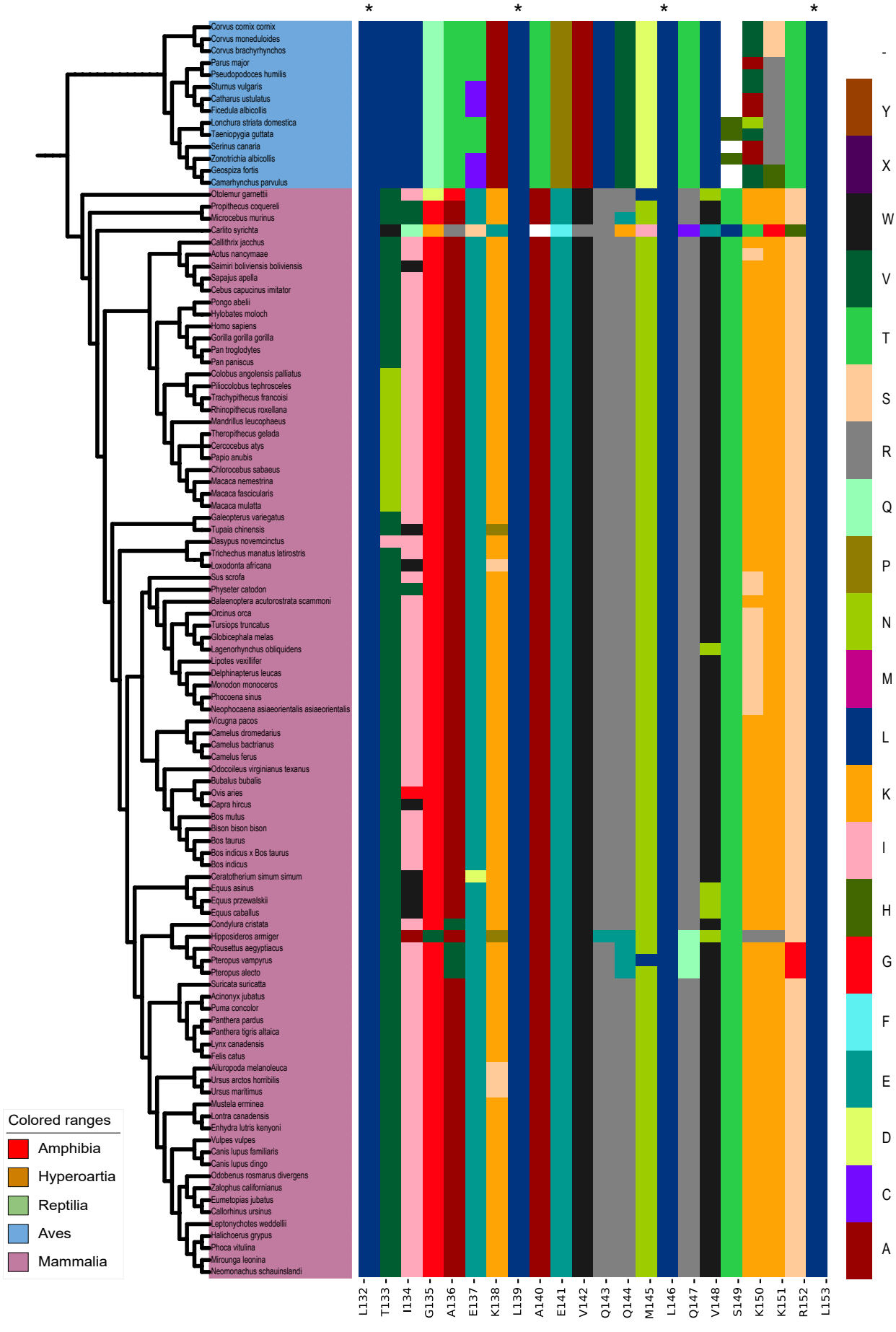
Corvus cornix cornix
Corvus monedulioides
Corvus brachyrhynchos
Parus major
Pseudopodoces humilis
Sturnus vulgaris
Catharus ustulatus
Ficedula albicollis
Lonchura striata domestica
Taeniopygia guttata
Serinus canaria
Zonotrichia albicollis
Geospiza fortis
Camarhynchus parvulus
Otolemur garnettii
Propithecus coquereli
Microcebus murinus
Carlito syrichta
Callithrix jacchus
Aotus nancymaae
Saimiri boliviensis boliviensis
Sapajus apella
Cebus capucinus imitator
Pongo abelii
Hylobates moloch
Homo sapiens
Gorilla gorilla gorilla
Pan troglodytes
Pan paniscus
Colobus angolensis palliatus
Piliocolobus tephrosceles
Trachypithecus francoisi
Rhinopithecus roxellana
Mandrillus leucophaeus
Theropithecus gelada
Cercocebus atys
Papio anubis
Chlorocebus sabaeus
Macaca nemestrina
Macaca fascicularis
Macaca mulatta
Galeopterus variegatus
Tupaia chinensis
Dasypus novemcinctus
Trichechus manatus latirostris
Loxodonta africana
Sus scrofa
Physeter catodon
Balaenoptera acutorostrata scammoni
Orcinus orca
Tursiops truncatus
Globicephala melas
Lagenorhynchus obliquidens
Lipotes vexillifer
Delphinapterus leucas
Monodon monoceros
Phocoena sinus
Neophocaena asiaeorientalis asiaeorientalis
Vicugna pacos
Camelus dromedarius
Camelus bactrianus
Camelus ferus
Odocoileus virginianus texanus
Bubalus bubalis
Ovis aries
Capra hircus
Bos mutus
Bison bison bison
Bos taurus
Bos indicus x Bos taurus
Bos indicus
Ceratotherium simum simum
Equus asinus
Equus przewalskii
Equus caballus
Condylura cristata
Hipposideros armiger
Rousettus aegyptiacus
Pteropus vampyrus
Pteropus alecto
Suricata suricatta
Acinonyx jubatus
Puma concolor
Panthera pardus
Panthera tigris altaica
Lynx canadensis
Felis catus
Ailuropoda melanoleuca
Ursus arctos horribilis
Ursus maritimus
Mustela erminea
Lontra canadensis
Enhydra lutris kenyoni
Vulpes vulpes
Canis lupus familiaris
Canis lupus dingo
Odobenus rosmarus divergens
Zalophus californianus
Eumetopias jubatus
Callorhinus ursinus
Leptonychotes weddellii
Halichoerus grypus
Phoca vitulina
Mirounga leonina
Neomonachus schauinslandi
Colored ranges
Amphibia
Hyperoartia
Reptilia
Aves
Mammalia
L132
T133
I134
G135
A136
E137
K138
L139
A140
E141
V142
Q143
Q144
M145
L146
Q147
V148
S149
K150
K151
R152
L153
-
Y
X
W
V
T
S
R
Q
P
N
M
L
K
I
H
G
F
E
D
C
A

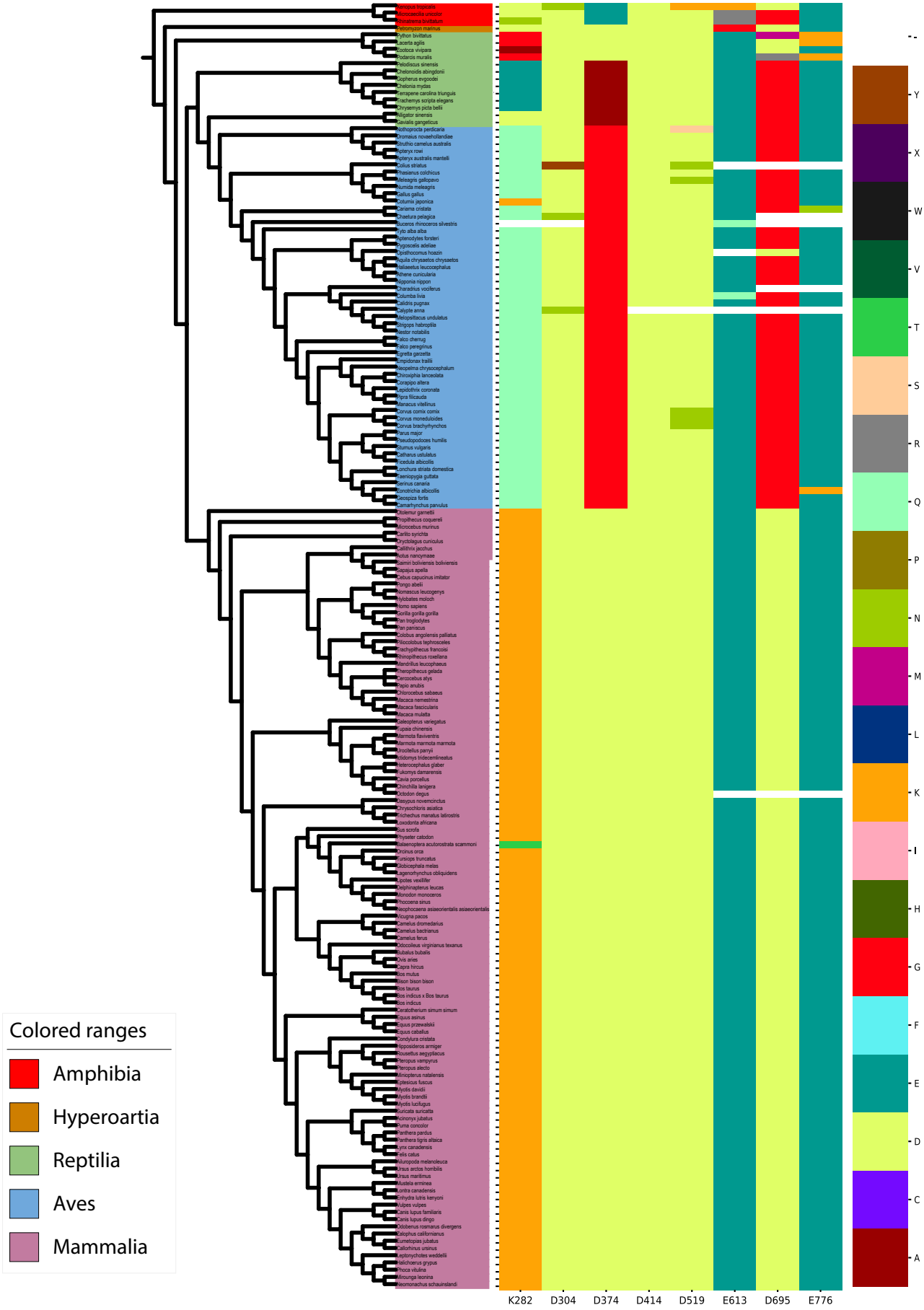
Colored ranges
Amphibia
Hyperoartia
Reptilia
Aves
Mammalia
K282
D304
D374
D414
D519
E613
D695
E776
-
Y
X
W
V
T
S
R
Q
P
N
M
L
K
I
H
G
F
E
D
C
A

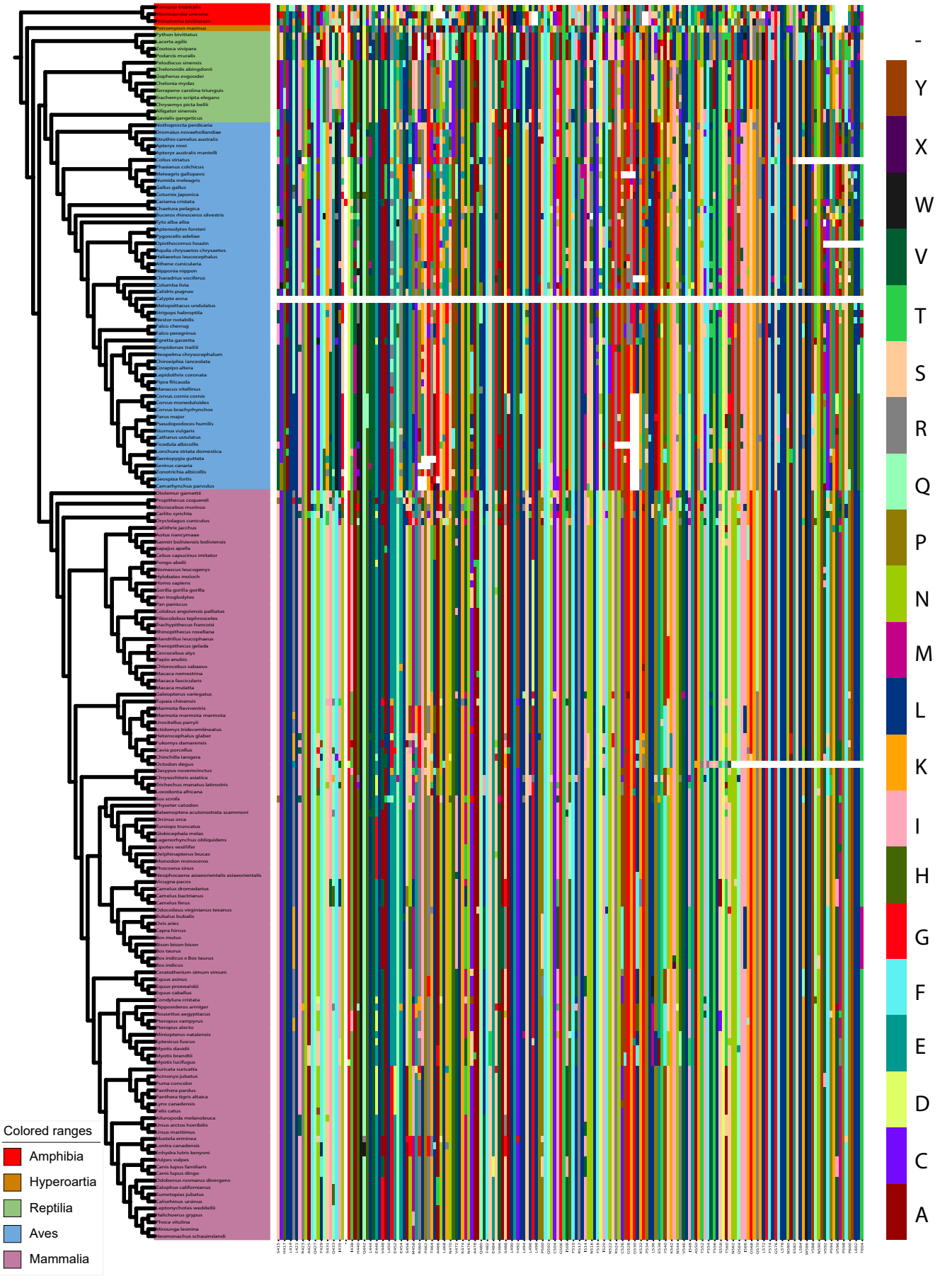
Colored ranges
Amphibia
Hyperoartia
Reptilia
Aves
Mammalia
-
Y
X
W
V
T
S
R
Q
P
N
M
L
K
I
H
G
F
E
D
C
A

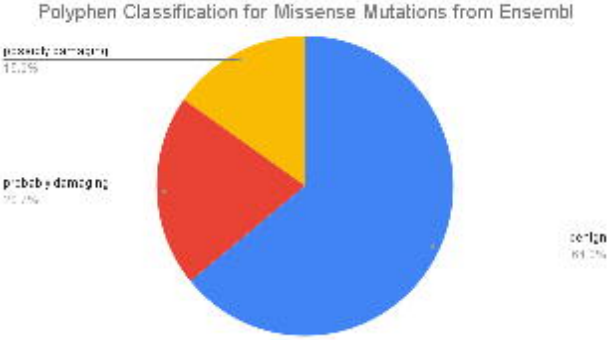
Polyphen Classification for Missense Mutations from Ensembl
possibly damaging
probably damaging
benign

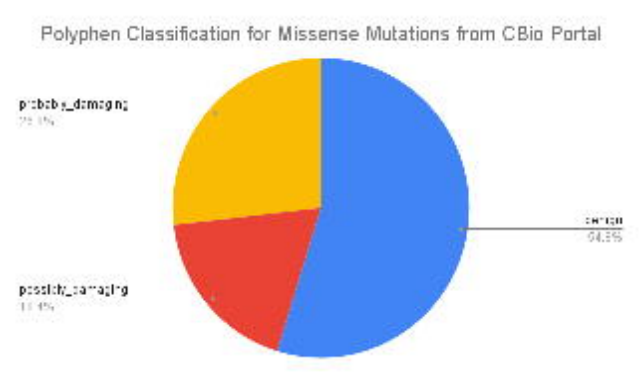
Polyphen Classification for Missense Mutations from CBio Portal
probably_damaging
benign
possibly_damaging

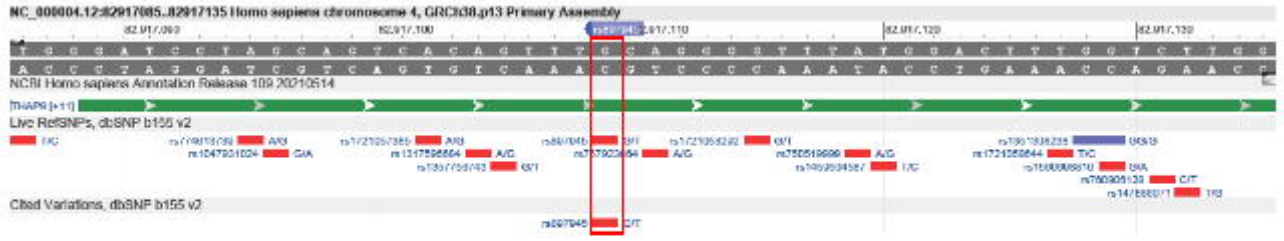
NC_000004.12:82917085..82917135 Homo sapiens chromosome 4, GRCh38.p13 Primary Assembly
NCBI Homo sapiens Annotation Release 109.20210514
Live RefSNPs, dbSNP b155 v2
Cited Variations, dbSNP b155 v2

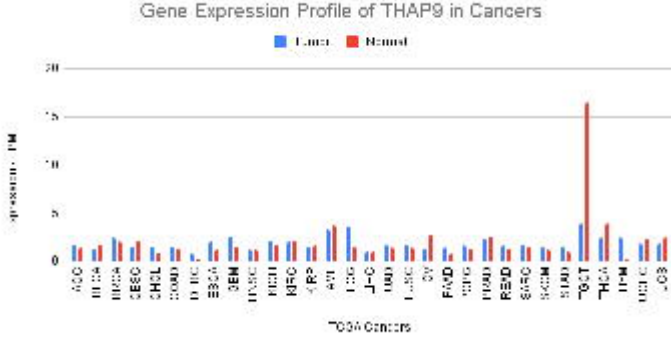
Gene Expression Profile of THAP9 in Cancers
Tumor
Normal
20
15
10
5
0
ACC
BLCA
BRCA
CESC
CHOL
COAD
DLBC
ESCA
GBM
HNSC
KICH
KIRC
KIRP
LAML
LGG
LIHC
LUAD
LUSC
MESO
OV
PAAD
PCPG
PRAD
READ
SARC
SKCM
STAD
TGCT
THCA
THYM
UCEC
UCS
UVM
TCGA Cancers

Figure 1: Phylogenetic analysis of THAP9 orthologs. (a) Phylogenetic tree of aligned protein sequences of THAP9 orthologs. Protein sequences were aligned using CLUSTALW[13], followed by building Maximum likelihood Phylogenetic trees[45] with 100 bootstrap replicates. **(b) Phylogenetic tree of aligned coding DNA sequences of THAP9 orthologs.** Coding DNA sequences of the THAP9 orthologs were codon aligned using PAL2NAL[16] and Maximum likelihood. Phylogenetic trees were generated using MEGAX[14] with 100 bootstrap replicates. The trees were generated using iTOL[17], and the organism classes are marked in different colors (legend on the left). Bootstrap values are marked on the tree.

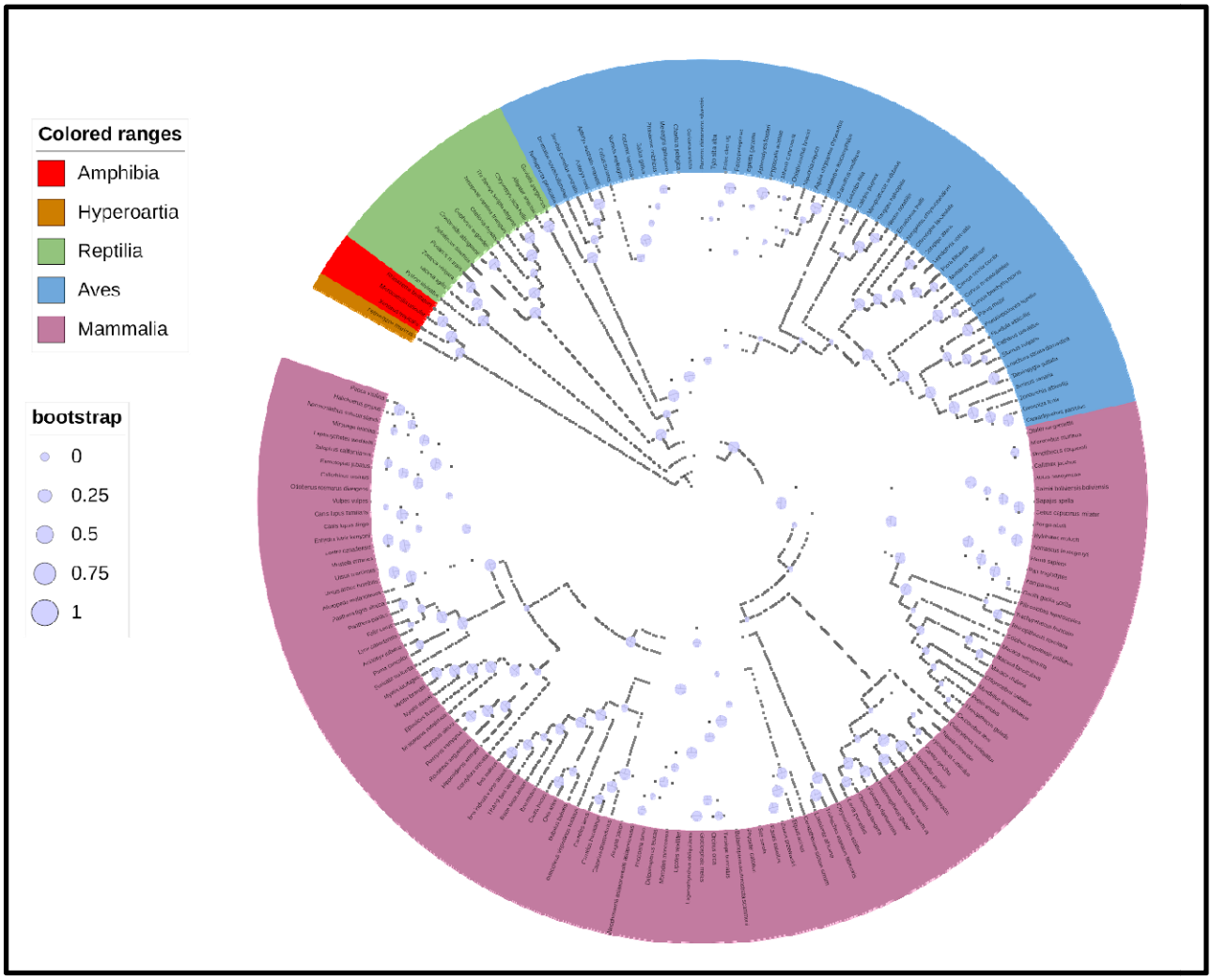

(a)

(b)

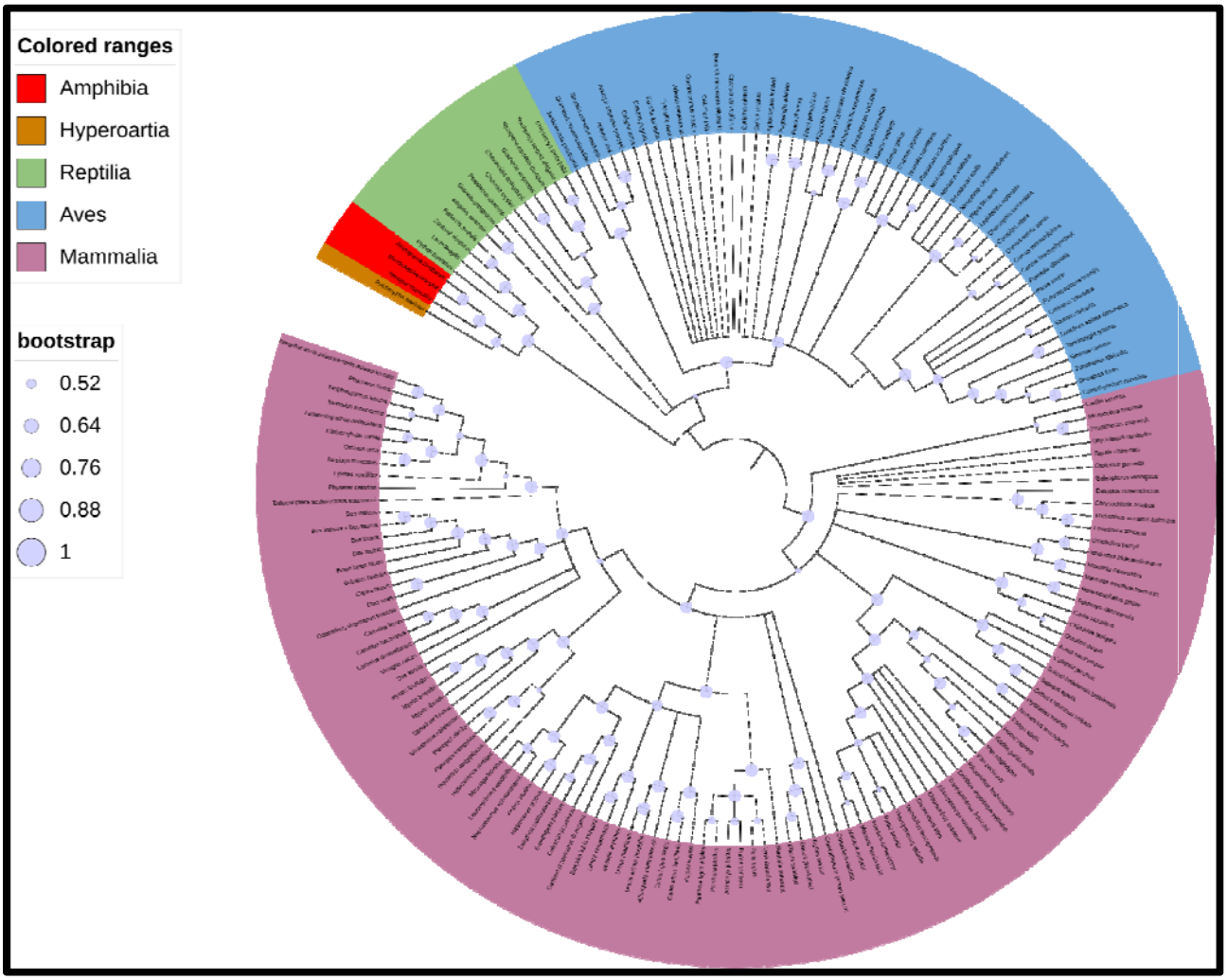
Colored ranges
Amphibia
Hyperoartia
Reptilia
Aves
Mammalia
bootstrap
0.52
0.64
0.76
0.88
1

Figure 2: Analysis of Selective Pressure Applied on THAP9 gene. Three independent analyses were performed using HyPhy-FEL[22], HyPhy-FUBAR[23], and HyPhy-MEME[24] packages. Significance was assessed by posterior probability > 0.9 (FUBAR) and p-value < 0.1 (MEME) and p-value < 0.1 (FEL).**(a)** FEL predicted 8 diversifying sites and 514 purifying selected sites. **(b)** FUBAR predicted 1 diversifying selected site and 618 purifying sites. **(c)** MEME observed 197 codon sites, distributed across the hTHAP9, to be evolved under episodic diversifying selection.

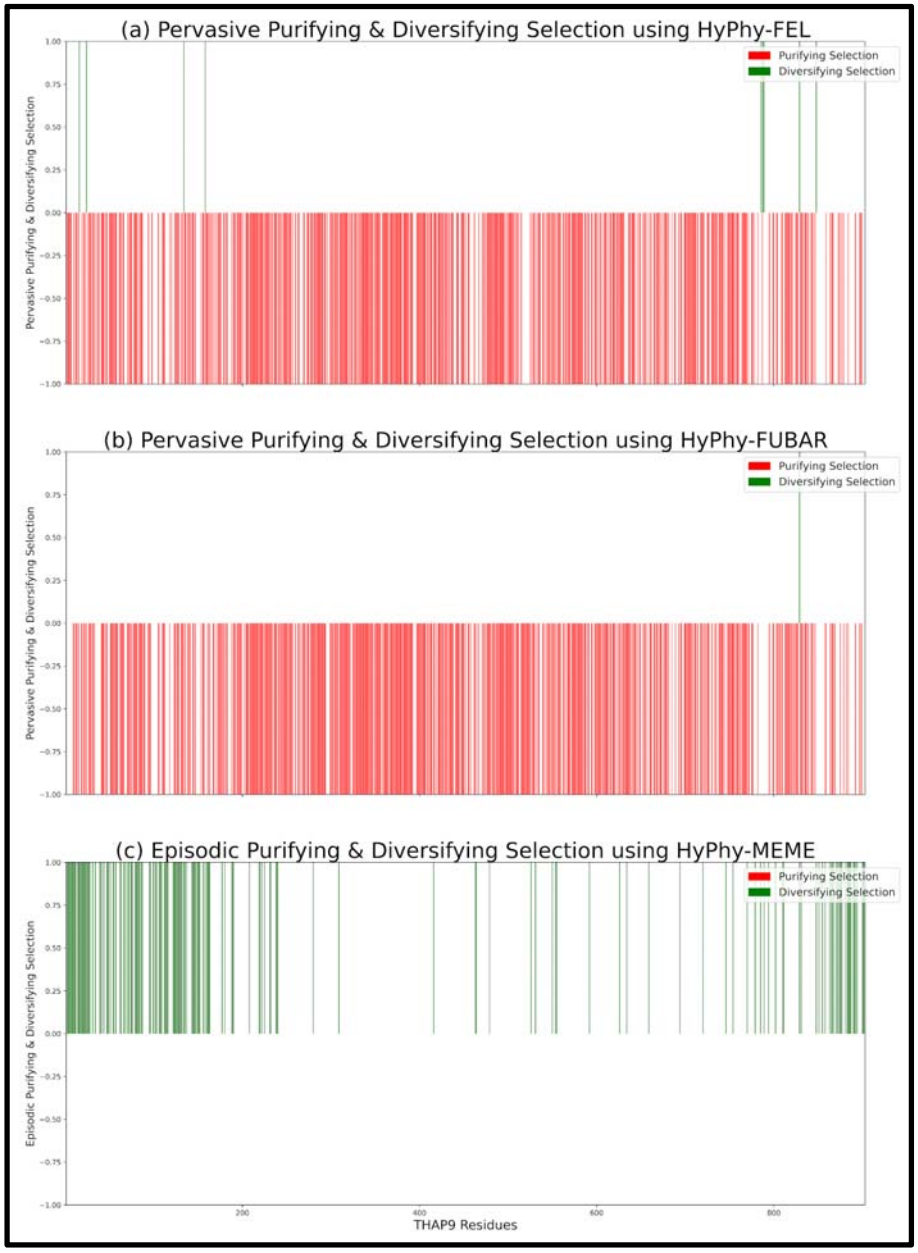

Figure 3: Amino Acid composition of human THAP9 protein.

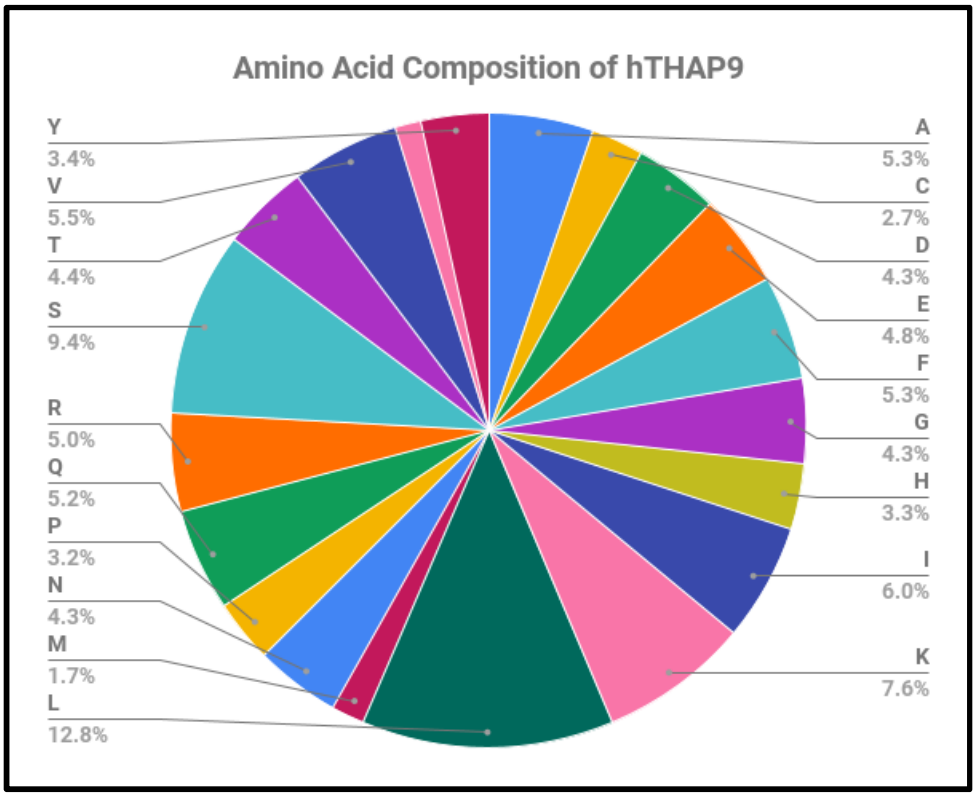

Figure 4: Previously annotated SMART[26] & Pfam[27] domains of THAP9 orthologs. Results were visualized on a phylogenetic tree using iTOL[17]. Domain architectures were displayed using the data export feature of SMART.

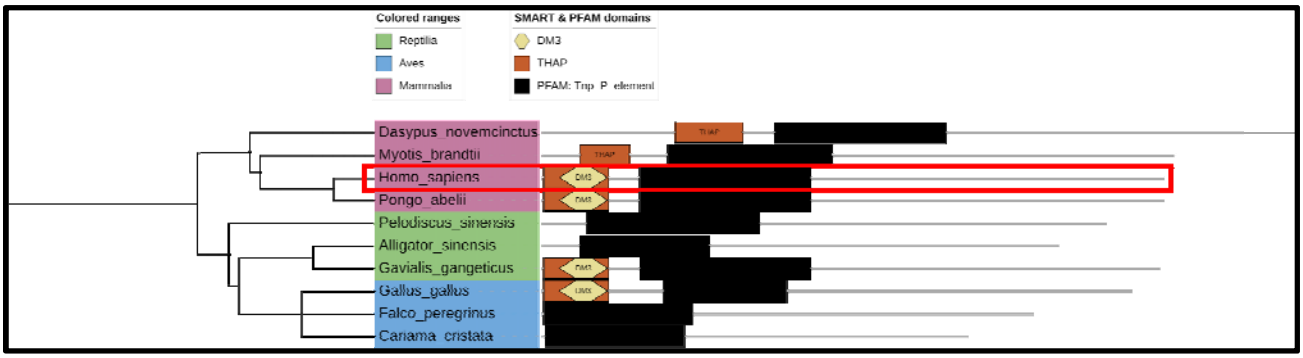

Figure 5: New predicted functional features **of THAP9 orthologs.** using Eukaryotic Linear Motif[28] (ELM) and ScanProsite[30] . The tree was made using iTOL[17].

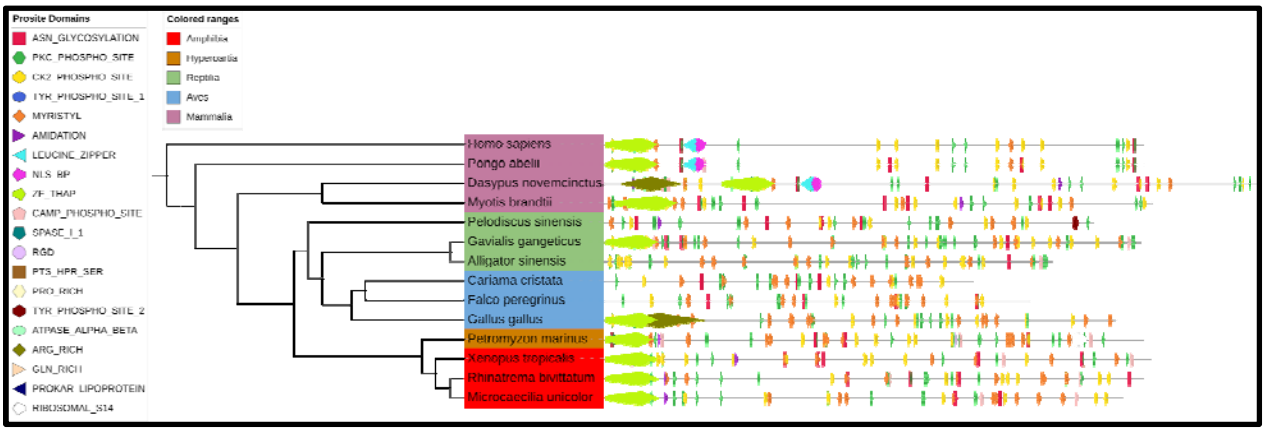

Figure 6: Architecture of N terminal (1-175) region hTHAP9. Predicted N-myristoylation sites (PS00008) (i) "GAilCS" (residues 58-63), (ii) "GAvpSV" (residues 83-88), and (iii) "GVsvTK"(residues 679-684). Predicted 4 adjacent motifs (i) "NYSL" N-glycosylation site (PS00001) (125-128) (ii) "SIK" Protein kinase C phosphorylation site (PS00005) (127-129) (iii) “LtigaekLaevqqmLqvskkrL” Leucine zipper pattern (PS00029) (132-153) (iv) “KRLISVKNYR-MIKKRK" Bipartite nuclear localization signal profile (PS50079) (151-166). This figure has been created using TBtools[51].

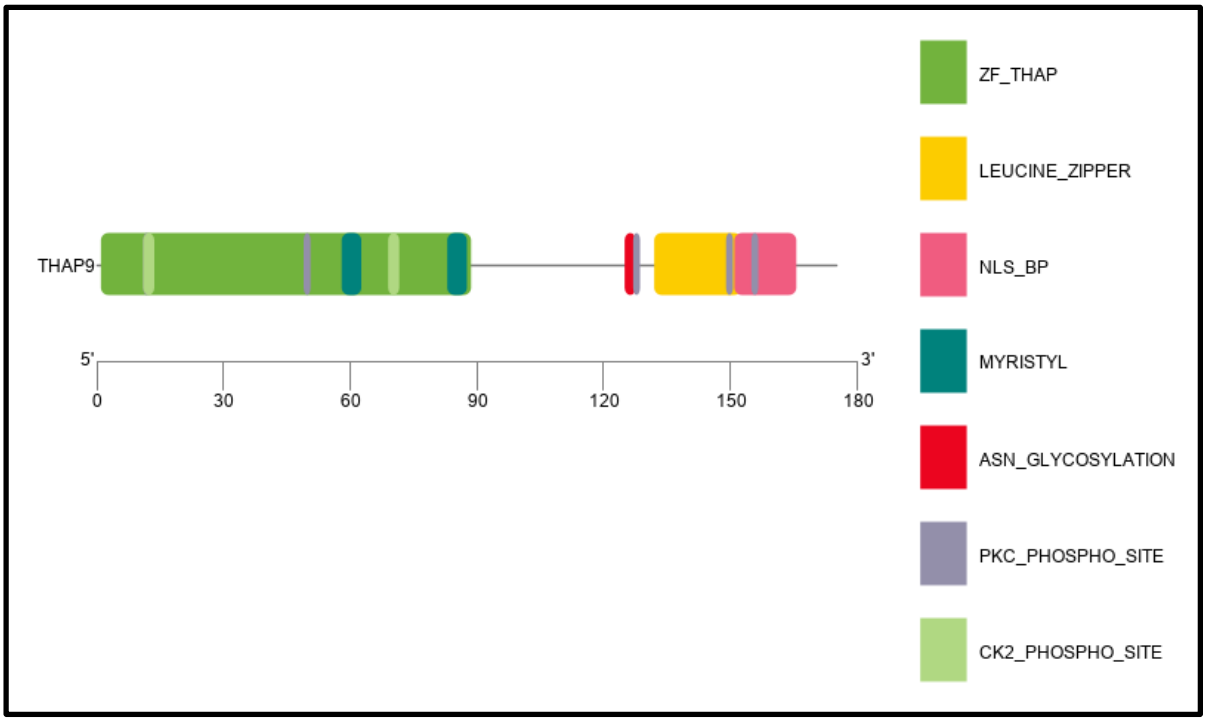

Figure 7: Top 30 MEME Motifs from THAP9 Ortholog Proteins. Schematic distribution of top 30 conserved motifs predicted in protein sequences of THAP9 orthologs. Motif analysis of 173 sequences was performed using MEME-suite[29]. The phylogenetic tree was constructed using the Maximum likelihood method available in MEGAX[45]. The trees were generated using iTOL[17], and the organisms' classes are marked in different colors with the legend given on the left side.

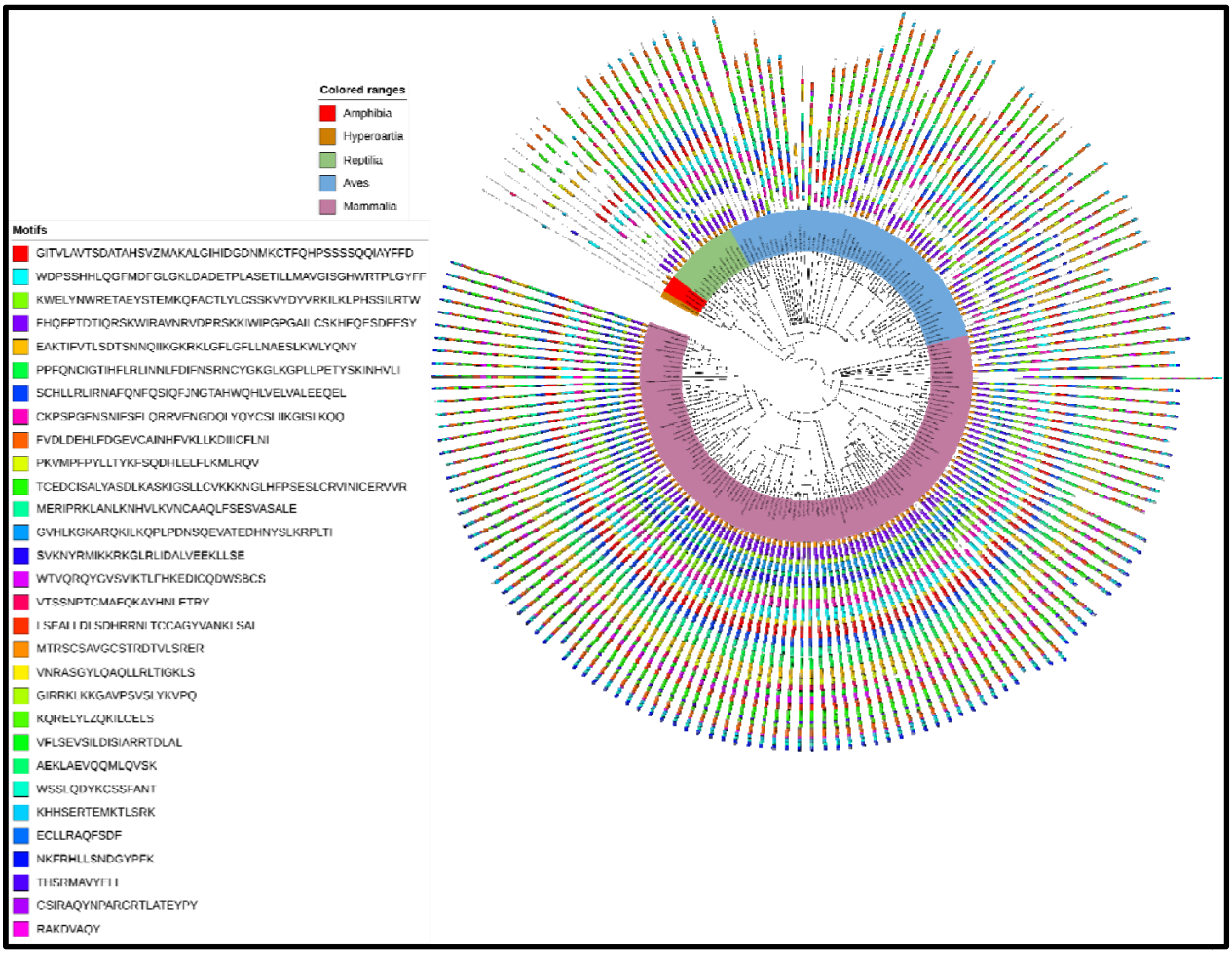

Figure 8: Evolution of THAP domain in THAP9 orthologs. Conserved functional residues (C5, C10, C62, H65; P29, W38, V85, and P86 in hTHAP9) have been highlighted with a * mark at the top.

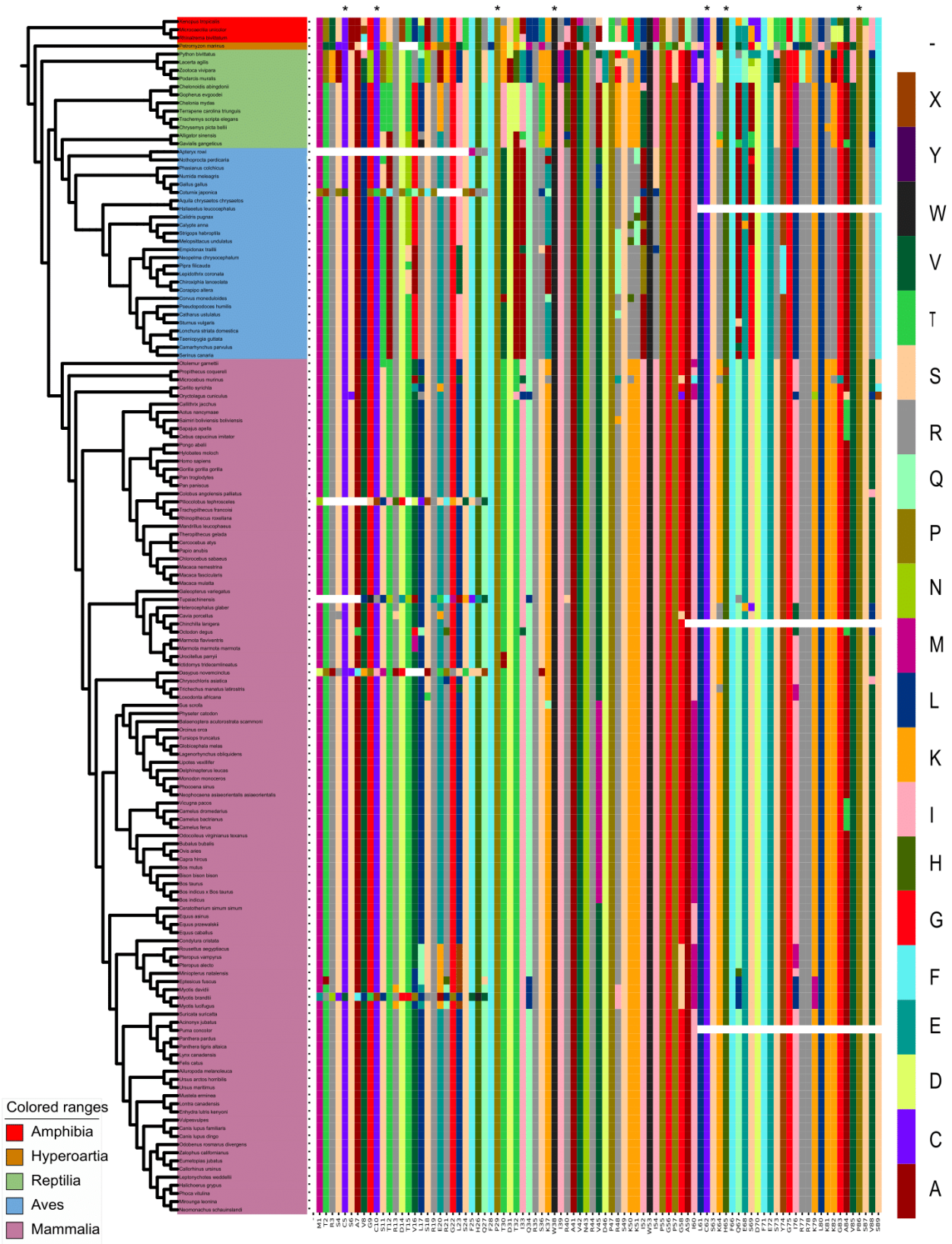
Colored ranges
Amphibia
Hyperoartia
Reptilia
Aves
Mammalia
-
X
Y
W
V
T
S
R
Q
P
N
M
L
K
I
H
G
F
E
D
C
A

Figure 9: Evolution of Leucine Zipper Domain in THAP9 orthologs. L132, L139, L146, and L153 (residue numbers correspond to hTHAP9) highlighted with *.

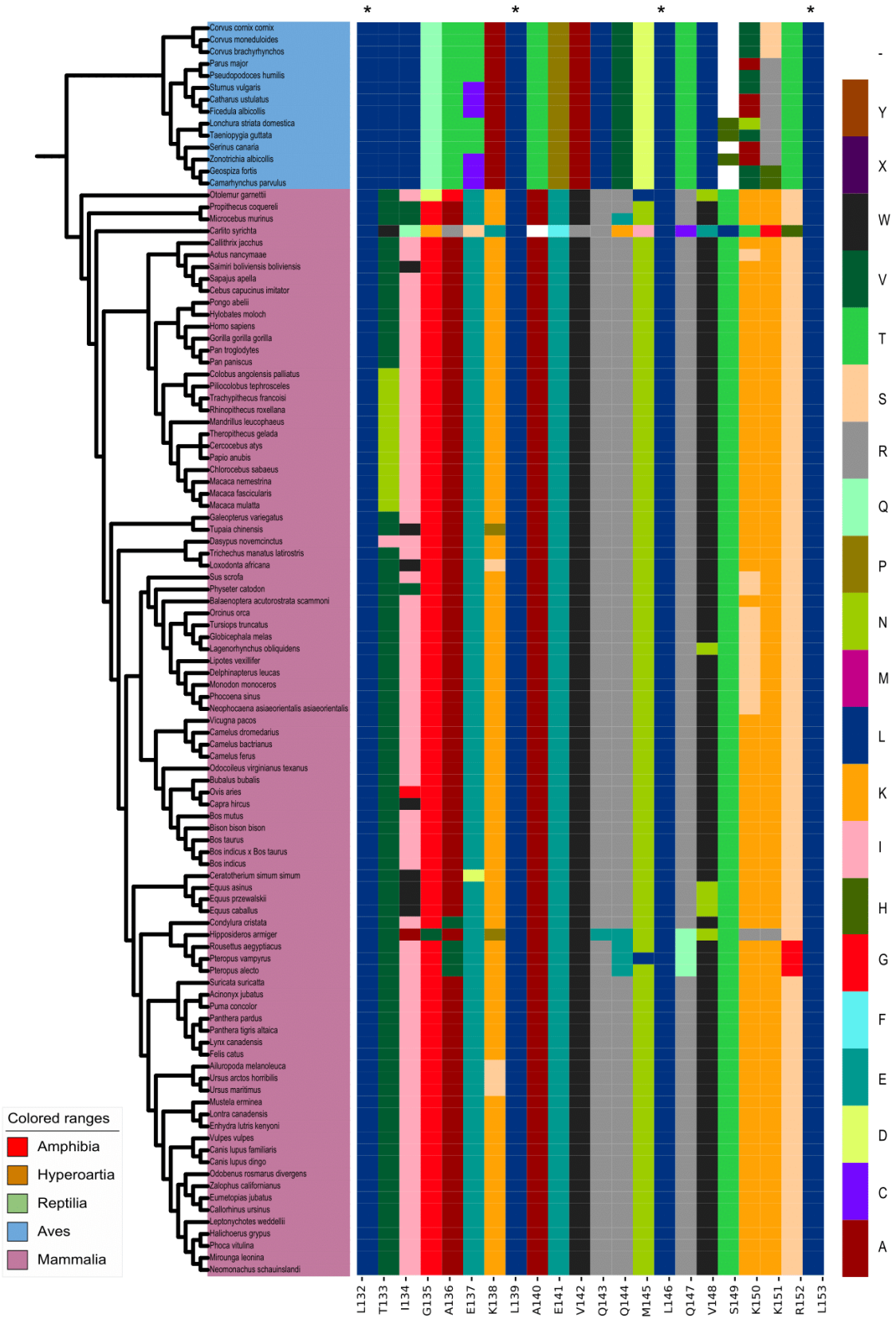
Corvus corax corax
Corvus monedulaoides
Corvus brachyrhynchos
Parus major
Pseudopodoces humilis
Sturnus vulgaris
Catharus ustulatus
Ficedula albicollis
Lonchura striata domestica
Taeniopygia guttata
Serinus canaria
Zonotrichia albicollis
Geospiza fortis
Camarhynchus parvulus
Otolemur garnettii
Propithecus coquereli
Microcebus murinus
Carlito syrichta
Callithrix jacchus
Aotus nancymaae
Saimiri boliviensis boliviensis
Sapajus apella
Cebus capucinus imitator
Pongo abelii
Hylobates moloch
Homo sapiens
Gorilla gorilla gorilla
Pan troglodytes
Pan paniscus
Colobus angolensis palliatus
Piliocolobus tephrosceles
Trachypithecus francoisi
Rhinopithecus roxellana
Mandrillus leucophaeus
Theropithecus gelada
Cercocebus atys
Papio anubis
Chlorocebus sabaeus
Macaca nemestrina
Macaca fascicularis
Macaca mulatta
Galeopterus variegatus
Tupaia chinensis
Dasypus novemcinctus
Trichechus manatus latirostris
Loxodonta africana
Sus scrofa
Physeter catodon
Balaenoptera acutorostrata scammoni
Orcinus orca
Tursiops truncatus
Globicephala melas
Lagenorhynchus obliquidens
Lipotes vexillifer
Delphinapterus leucas
Monodon monoceros
Phocoena sinus
Neophocaena asiaeorientalis asiaeorientalis
Vicugna pacos
Camelus dromedarius
Camelus bactrianus
Camelus ferus
Odocoileus virginianus texanus
Bubalus bubalis
Ovis aries
Capra hircus
Bos mutus
Bison bison bison
Bos taurus
Bos indicus x Bos taurus
Bos indicus
Ceratotherium simum simum
Equus asinus
Equus przewalskii
Equus caballus
Condylura cristata
Hipposideros armiger
Rousettus aegyptiacus
Pteropus vampyrus
Pteropus alecto
Suricata suricatta
Acinonyx jubatus
Puma concolor
Panthera pardus
Panthera tigris altaica
Lynx canadensis
Felis catus
Ailuropoda melanoleuca
Ursus arctos horribilis
Ursus maritimus
Mustela erminea
Lontra canadensis
Enhydra lutris kenyoni
Vulpes vulpes
Canis lupus familiaris
Canis lupus dingo
Odobenus rosmarus divergens
Zalophus californianus
Eumetopias jubatus
Callorhinus ursinus
Leptonychotes weddellii
Halichoerus grypus
Phoca vitulina
Mirounga leonina
Neomonachus schauinslandi
Colored ranges
Amphibia
Hyperoartia
Reptilia
Aves
Mammalia
L132
T133
I134
G135
A136
E137
K138
L139
A140
E141
V142
Q143
Q144
M145
L146
Q147
V148
S149
K150
K151
R152
L153
-
Y
X
W
V
T
S
R
Q
P
N
M
L
K
I
H
G
F
E
D
C
A

Figure 10: Evolution of catalytic residues of the RNaseH-like catalytic domain in THAP9 orthologs. D304, D374, D414, D519, E613, D695 & E776 are the important catalytic residues of hTHAP9[55].

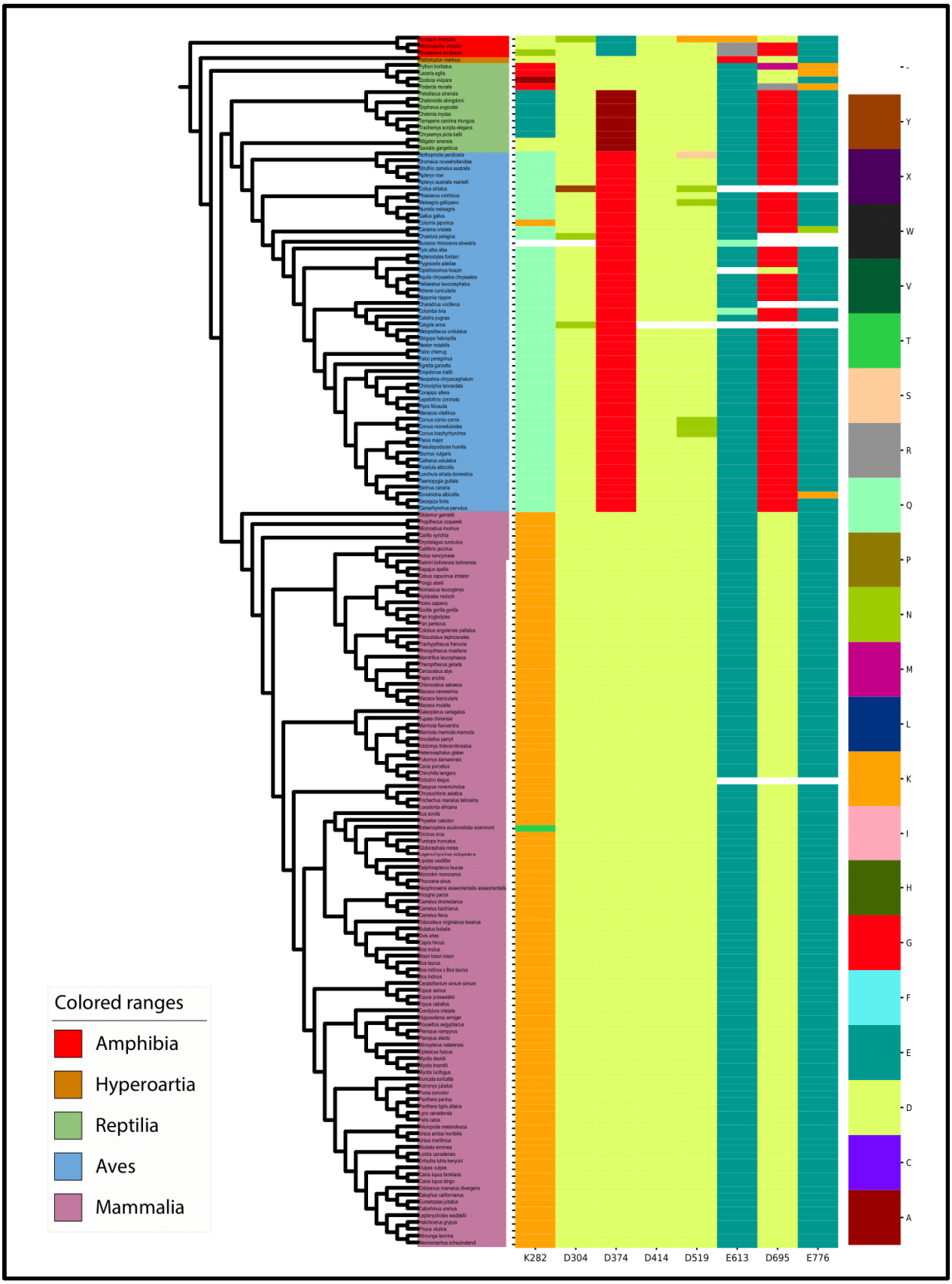
Colored ranges
Amphibia
Hyperoartia
Reptilia
Aves
Mammalia
K282
D304
D374
D414
D519
E613
D695
E776
Y
X
W
V
T
S
R
Q
P
N
M
L
K
I
H
G
F
E
D
C
A

Figure 11: Evolution of predicted insertion domain in THAP9 orthologs.

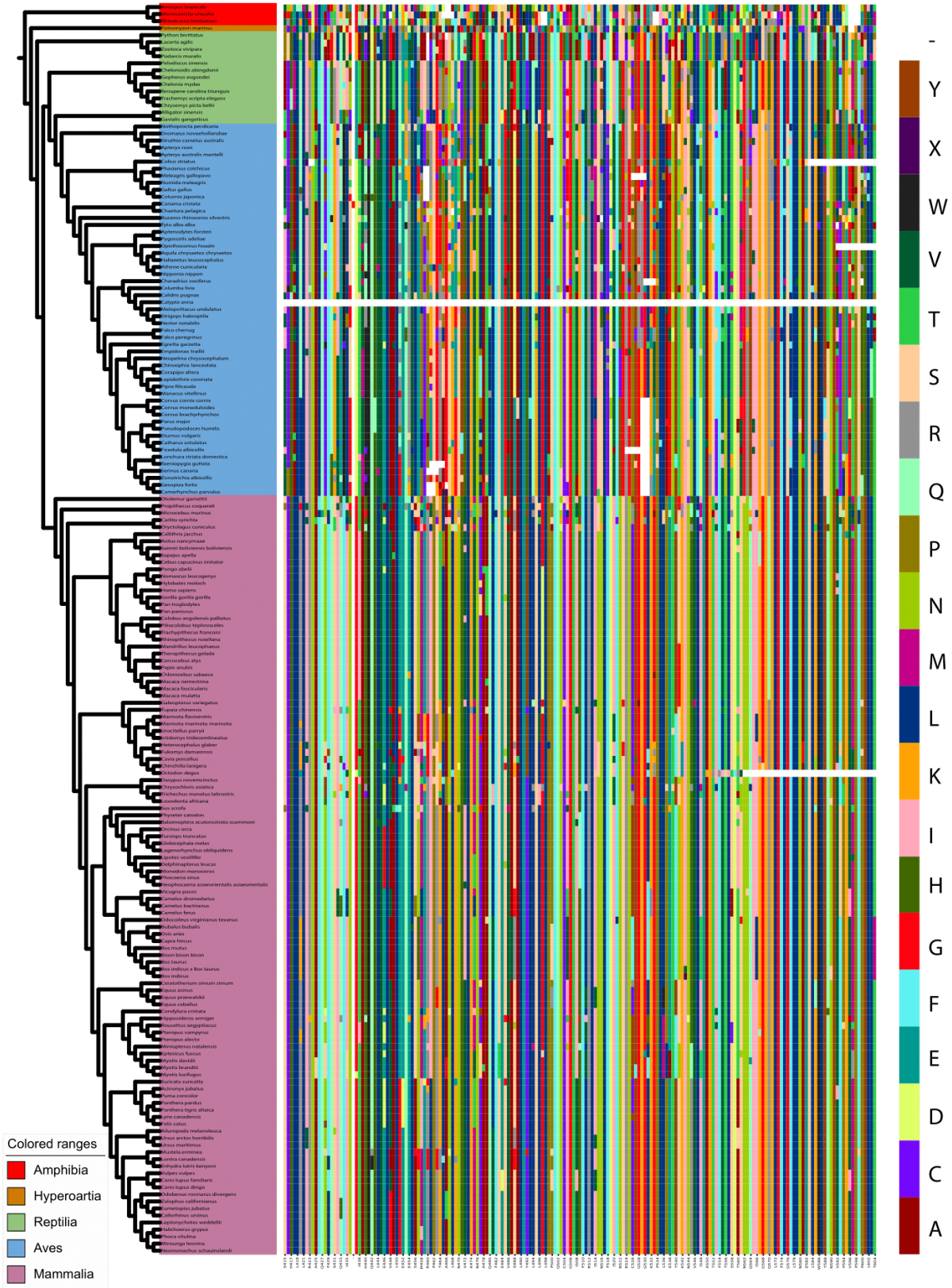
Colored ranges
Amphibia
Hyperoartia
Reptilia
Aves
Mammalia
-
Y
X
W
V
T
S
R
Q
P
N
M
L
K
I
H
G
F
E
D
C
A

Figure 12: PolyPhen classification for Missense Mutations from Ensembl. PolyPhen classification of 820 Missense SNPs of human THAP9 gene (from Ensembl) into benign, possibly- damaging, and probably damaging categories.

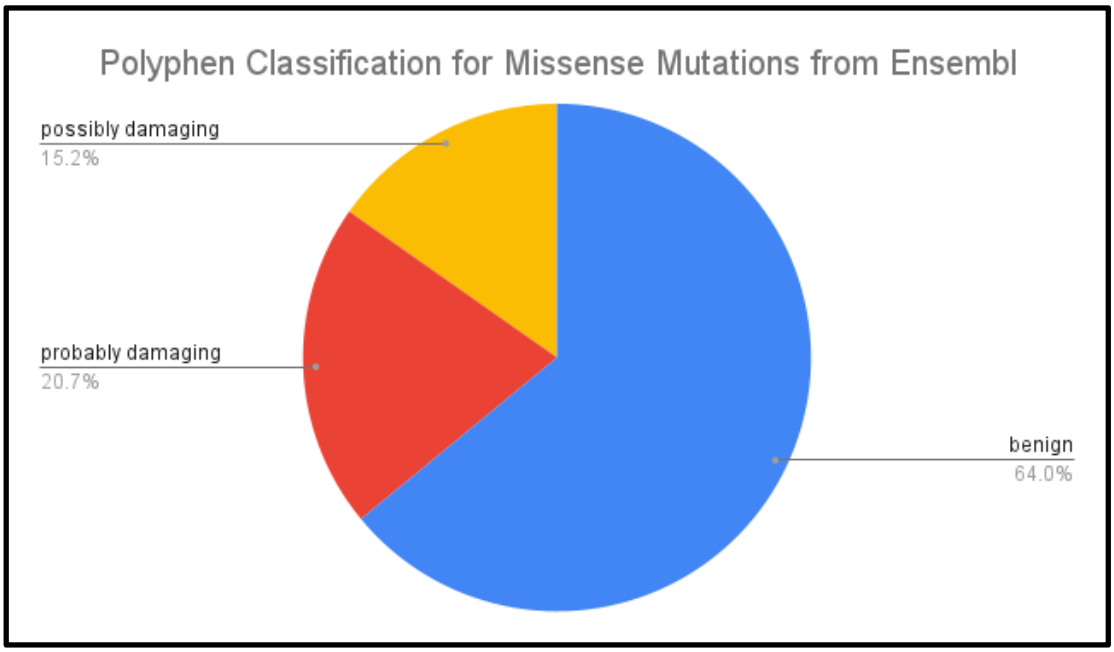

Figure 13: PolyPhen classification for Missense Mutations from CBio Portal. PolyPhen classification of 272 Missense SNPs of human THAP9 gene (from cBio Portal) into benign, possibly- damaging, and probably damaging categories.

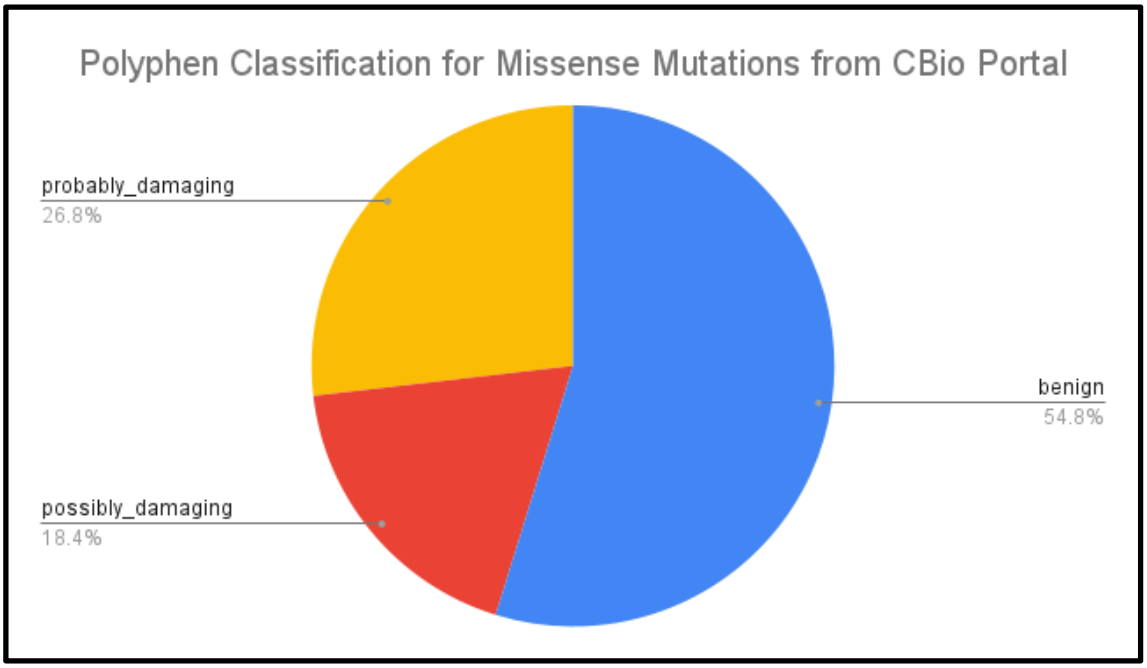

Figure 14: Genome Variation Viewer view of rs897945. rs897945 yields a G→T nucleotide substitution which leads to Leucine to Phenylalanine amino acid change at position 299 located on the Tnp_P_element (Pfam ID: PF12017) domain in hTHAP9 protein.

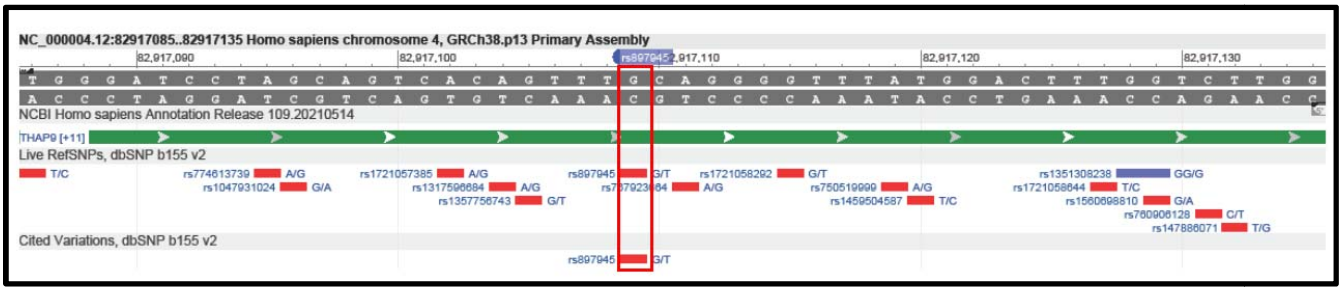

Figure 15: Gene Expression Profile of THAP9 in Cancers. The pan-cancer expression profile of THAP9 has been plotted using the GEPIA tool, which used cancer and matched normal from TCGA and GTEx portal. Pan-cancer view of THAP9 expression showed overexpression of THAP9 in Testicular Cancer (TGCT) and reduced expression of THAP9 in Thymic Epithelial Tumors (THYM). ACC, adrenocortical carcinoma; BLCA, bladder urothelial carcinoma; BRCA, breast invasive carcinoma; CESC, cervical and endocervical cancers; CHOL, cholangiocarcinoma; COAD, colon adenocarcinoma; DLBC, lymphoid neoplasm diffuse large B-cell lymphoma; ESCA, esophageal carcinoma; GBM, glioblastoma multiforme; HNSC, head and neck squamous cell carcinoma; KICH, kidney chromophobe; KIRC, kidney renal clear cell carcinoma; KIRP, kidney renal papillary cell carcinoma; LAML, acute myeloid leukemia; LGG, brain lower grade glioma; LIHC, liver hepatocellular carcinoma; LUAD, lung adenocarcinoma; LUSC, lung squamous cell carcinoma; MESO, mesothelioma; OV, ovarian serous cystadenocarcinoma; PAAD, pancreatic adenocarcinoma; PCPG, pheochromocytoma and paraganglioma; PRAD, prostate adenocarcinoma; READ, rectum adenocarcinoma; SARC, sarcoma; SKCM, skin cutaneous melanoma; STAD, stomach adenocarcinoma; STES, stomach and esophageal carcinoma; TGCT, testicular germ cell tumors; THCA, thyroid carcinoma; THYM, thymoma; UCEC, uterine corpus endometrial carcinoma; UCS, uterine carcinosarcoma; UVM, uveal melanoma.

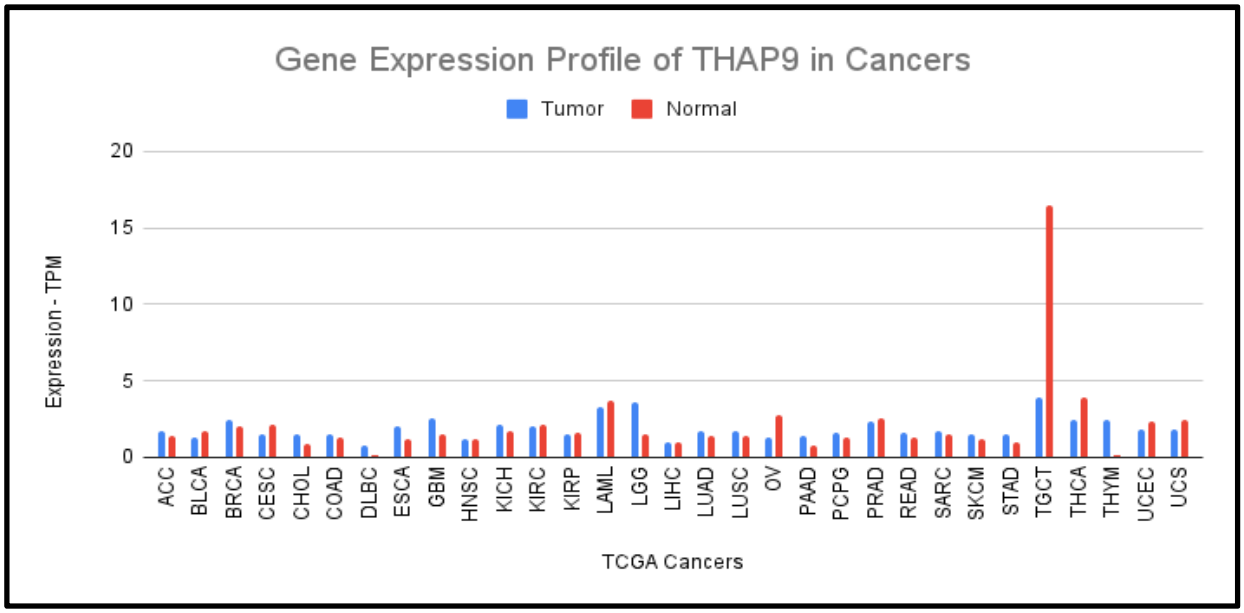

Supplementary Figure 1: (a) Full tree representation of previously annotated SMART & Pfam domains of THAP9 orthologs. Results were visualized on a phylogenetic tree using iTOL. Domain architectures were displayed using the data export feature of SMART. **(b) Full tree representation of newly predicted features of THAP9 orthologs** using Eukaryotic Linear Motif (ELM) and ScanProsite.

(a)

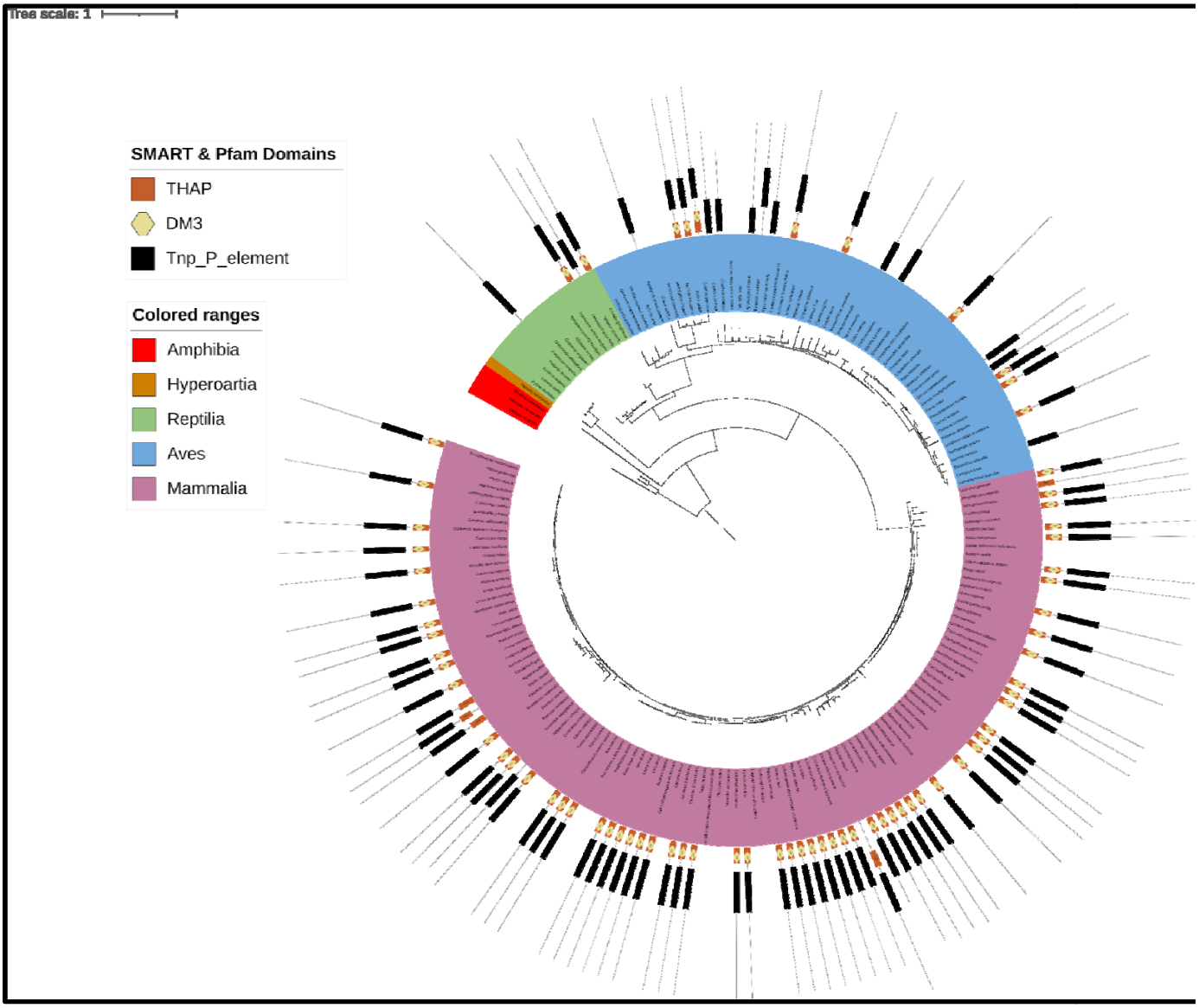

(b)

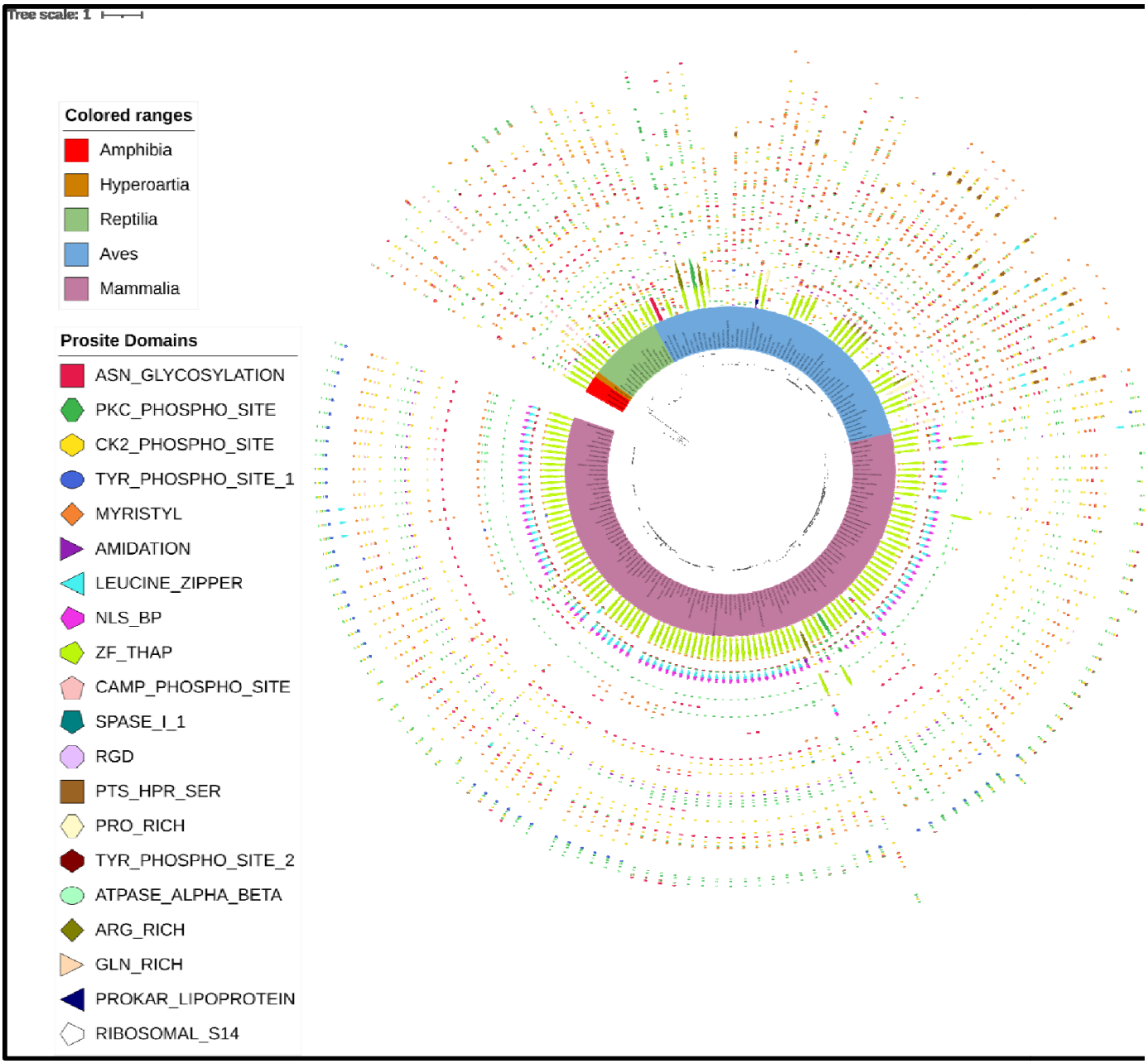
Tree scale: 1
Colored ranges
Amphibia
Hyperoartia
Reptilia
Aves
Mammalia
Prosite Domains
ASN_GLYCOSYLATION
PKC_PHOSPHO_SITE
CK2_PHOSPHO_SITE
TYR_PHOSPHO_SITE_1
MYRISTYL
AMIDATION
LEUCINE_ZIPPER
NLS_BP
ZF_THAP
CAMP_PHOSPHO_SITE
SPASE_I_1
RGD
PTS_HPR_SER
PRO_RICH
TYR_PHOSPHO_SITE_2
ATPASE_ALPHA_BETA
ARG_RICH
GLN_RICH
PROKAR_LIPOPROTEIN
RIBOSOMAL_S14